NAVAL POSTGRADUATE SCHOOL

MONTEREY, CALIFORNIA

THESIS

THE ROLE OF STRESS IN THE CORROSION CRACKING OF ALUMINUM ALLOYS

By

Brian E-S. Scott

March 2013

Thesis Advisor:	Luke, N. Brewer
Second Reader:	Young, W. Kwon

THIS PAGE INTENTIONALLY LEFT BLANK

REPORT DOCUMENTATION PAGE			Form Approved OMB No. 0704-0188
Public reporting burden for this collection of information is estimated to average 1 hour per response, including the time for reviewing instruction, searching existing data sources, gathering and maintaining the data needed, and completing and reviewing the collection of information. Send comments regarding this burden estimate or any other aspect of this collection of information, including suggestions for reducing this burden, to Washington headquarters Services, Directorate for Information Operations and Reports, 1215 Jefferson Davis Highway, Suite 1204, Arlington, VA 22202-4302, and to the Office of Management and Budget, Paperwork Reduction Project (0704-0188) Washington DC 20503.			
1. AGENCY USE ONLY ***(Leave blank)***	**2. REPORT DATE** March 2013	**3. REPORT TYPE AND DATES COVERED** Master's Thesis	
4. TITLE AND SUBTITLE THE ROLE OF STRESS IN THE CORROSION CRACKING OF ALUMINUM ALLOYS		**5. FUNDING NUMBERS**	
6. AUTHOR(S) Brian E-S. Scott			
7. PERFORMING ORGANIZATION NAME(S) AND ADDRESS(ES) Naval Postgraduate School Monterey, CA 93943-5000		**8. PERFORMING ORGANIZATION REPORT NUMBER**	
9. SPONSORING /MONITORING AGENCY NAME(S) AND ADDRESS(ES) N/A		**10. SPONSORING/MONITORING AGENCY REPORT NUMBER**	
11. SUPPLEMENTARY NOTES The views expressed in this thesis are those of the author and do not reflect the official policy or position of the Department of Defense or the U.S. Government. IRB Protocol number ____N/A____.			
12a. DISTRIBUTION / AVAILABILITY STATEMENT Approved for public release;distribution is unlimited		**12b. DISTRIBUTION CODE**	

13. ABSTRACT (maximum 200 words)

This work examines the effect of stress on the rate of sensitization, the rate of pitting corrosion and the rate of crack nucleation of aluminum alloy 5083-H116 aluminum. Stress corrosion cracking in aluminum superstructures of Naval vessels is a multibillion-dollar maintenance problem, which requires more scientific understanding to better predict and mitigate. To investigate the role of applied stress on these corrosion-related processes, rolled plate of AA5083 was placed under tensile stress through bending while being subject to elevated temperature and salt spray. Nitric acid mass loss tests quantified the amount of sensitization as a function of stress level. Optical micrographs were used to determine the rate of pitting corrosion and crack nucleation while under applied tensile stress. The effect of applied, elastic stress on the degree of sensitization was inconclusive. Applied stress did increase the rate of localized corrosion, in terms of both pitting and intergranular corrosion. Moreover, the orientation of the plate with respect to the applied tensile stress, strongly affected the type and amount of localized corrosion observed. When the tensile stress was applied across the rolling direction, more localized corrosion occurred and intergranular corrosion dominant over pitting.

14. SUBJECT TERMS Stress Corrosion Cracking, 5083 Aluminum Alloy			**15. NUMBER OF PAGES** 81
			16. PRICE CODE
17. SECURITY CLASSIFICATION OF REPORT Unclassified	**18. SECURITY CLASSIFICATION OF THIS PAGE** Unclassified	**19. SECURITY CLASSIFICATION OF ABSTRACT** Unclassified	**20. LIMITATION OF ABSTRACT** UU

NSN 7540-01-280-5500 Standard Form 298 (Rev. 2-89)
Prescribed by ANSI Std. 239-18

THIS PAGE INTENTIONALLY LEFT BLANK

Approved for public release;distribution is unlimited

THE ROLE OF STRESS IN THE CORROSION CRACKING OF ALUMINUM ALLOYS

Brian E-S. Scott
Lieutenant, United States Navy
B.S., Virginia Polytechnic Institute and State University, 2008

Submitted in partial fulfillment of the
requirements for the degree of

MASTER OF SCIENCE IN MECHANICAL ENGINEERING

from the

NAVAL POSTGRADUATE SCHOOL
March 2013

Author: Brian E-S. Scott

Approved by: Luke N. Brewer
Thesis Advisor

Young W. Kwon
Second Reader

Knox T. Millsaps
Chair, Department of Mechanical and Aerospace Engineering

THIS PAGE INTENTIONALLY LEFT BLANK

ABSTRACT

This work examines the effect of stress on the rate of sensitization, the rate of pitting corrosion and the rate of crack nucleation of aluminum alloy 5083-H116 aluminum. Stress corrosion cracking in aluminum superstructures of naval vessels is a multibillion-dollar maintenance problem, which requires more scientific understanding to better predict and mitigate. To investigate the role of applied stress on these corrosion-related processes, rolled plate of AA5083 was placed under tensile stress through bending while being subject to elevated temperature and salt spray. Nitric acid mass loss tests quantified the amount of sensitization as a function of stress level. Optical micrographs were used to determine the rate of pitting corrosion and crack nucleation while under applied tensile stress. The effect of applied, elastic stress on the degree of sensitization was inconclusive. Applied stress did increase the rate of localized corrosion, in terms of both pitting and intergranular corrosion. Moreover, the orientation of the plate with respect to the applied tensile stress, strongly affected the type and amount of localized corrosion observed. When the tensile stress was applied across the rolling direction, more localized corrosion occurred and intergranular corrosion was dominant over pitting.

THIS PAGE INTENTIONALLY LEFT BLANK

TABLE OF CONTENTS

LIST OF FIGURES

LIST OF TABLES

THIS PAGE INTENTIONALLY LEFT BLANK

LIST OF ACRONYMS AND ABBREVIATIONS

Required if thesis contains six or more.

IGC	Intergranular Corrosion
IGSCC	Intergranular Stress Corrosion Cracking
NAMLT	Nitric Acid Mass Loss Test
SCC	Stress Corrosion Cracking
TGSCC	Transgranular Stress Corrosion Cracking

THIS PAGE INTENTIONALLY LEFT BLANK

ACKNOWLEDGMENTS

First and foremost I would like to thank Professor Brewer for his unwavering support, passion for science and experimentation. He is always willing to go above and beyond for the advancement of his students. I have learned a lot not only about aluminum and stress corrosion cracking but also about the process of experimentation. Without his encouragement and leadership, this research would have been a lot less educational.

I would like to thank all the professors and staff of NPS who gave their time and knowledge, especially Dr. C. Park, and John Mobley.

We gratefully acknowledge financial support for this research from the OSD-Corrosion Policy and Oversight office and its Technical Corrosion Collaboration.

THIS PAGE INTENTIONALLY LEFT BLANK

I. INTRODUCTION AND BACKGROUND

A. MOTIVATION

For the past several decades, there has been a push to increase the efficiency of everything that we use. This trend also applies to ships, both commercial and military. With fuel costs increasing every year, the need arises to move larger loads with less fuel. In order to accomplish this goal, the shipbuilding industry has been using aluminum in ship structures for many years. There are many benefits to using aluminum for ship structures: aluminum is one-third of the density of steel, thus a ship using aluminum in its construction can be lighter than an all-steel ship. For commercial shipping, the dry weight of the ship can be reduced, allowing more cargo to be carried while burning the same amount of fuel; that in turn, increases the profit margins for the shipping company. In the military, the weight savings means that the ship can carry more ammunition and supplies, or that it can carry the same amount of ammunition and supplies but travel further distances at increased speeds.

Using aluminum instead of steel for the ship's superstructure construction will lower the ships center of gravity increasing the transverse stability of the ship. Increasing transverse stability allows the ship to be operated in higher sea states that would normally prohibit the safe operation of the ship. This is important for commercial shipping such as ferries, as, in order to be profitable, they need to operate day consistently despite the weather conditions. For larger ships such as container ships and oil tankers, increased stability means that instead of diverting around a storm (traveling further distances and burning more fuel), they can travel through the storm without jeopardizing the safety of the ship. For military ships using aluminum, especially in the topside superstructure, lowers the center of gravity of the ship, allowing the ship's beam to be narrower than normally possible. Therefore, the ship's hull form can be more slender, allowing the ship to cut through the water and travel faster and further while using less fuel and thus making the ship more combat effective. This is why the U.S Navy has used aluminum for the superstructure in the Ticonderoga class of cruisers and continues to use aluminum for the construction of the littoral combat ship which is constructed entirely of aluminum.

Marine grade aluminum alloys (Aluminum Association 5xxx series) have been and continue to be used for ship construction because of their specific strength and good general corrosion properties. While aluminum in its pure form is extremely corrosion resistant, its mechanical strength properties are low. In order for aluminum to have the strength necessary to be used for structural members, it is necessary to alloy aluminum with other metals. The primary alloying addition in 5000 series aluminum is magnesium, which gives the material good specific strength and general corrosion properties and is also easily weldable. Other series of aluminum, such as the 2000 series, use different alloying additions, such as copper, that provide greater specific strength; however, their resistance to corrosion is poor. Additionally, the 1000 series aluminum alloys have excellent corrosion resistance; however, their strength is not sufficient for use in ship structures. Therefore, the 5000 series aluminum alloys provide a good compromise between strength and general corrosion resistance. The general corrosion properties of 5000 series aluminum are good because of the passivating oxide film that forms on the surface of the aluminum; however, they are susceptible to a phenomenon known as stress corrosion cracking (SCC). SCC is a condition commonly associated with two main forms of cracking: transgranular stress corrosion cracking (TGSCC) and intergranular stress corrosion cracking (IGSCC) [1].

Aluminum alloys of the 5000 series are most susceptible to IGSCC, where cracks propagate along the grain boundaries between individual grains, as opposed to TGSCC, where cracks travel across the grains. This problem is most prevalent in the Ticonderoga (CG-47) class of cruisers that use AA5456 [2]; however similar issues have been observed in civilian ships using the related alloy AA5083 [3]. The magnesium, when used in solid solution, increases the strength of the material. When the concentration of magnesium increases to above 3 wt.%, as is the case with AA5456 (5.1wt%) and AA5083 (4.7wt%), and is exposed to elevated temperatures for prolonged periods of time, the magnesium will come out of solution and diffuse to the grain boundaries forming β-phase (Mg_2Al_3) [2]. This effect is called sensitization, and once this process occurs, the material becomes susceptible to IGSCC. When sensitized and combined with

a corrosive environment such as seawater and the presence of a tensile stress from either welding or structural loading, IGSCC will occur.

B. STRESS CORROSION CRACKING (SCC)

For IGSCC to happen, three factors need to be in place: the material must be sufficiently sensitized, a tensile stress must be present, and the material must be in a corrosive environment. Sensitization in aluminum alloy 5083 occurs when the aluminum is subjected to temperatures higher than 50°C (122°F) [4]. It is not uncommon for the exposed portions of the superstructure to reach these temperatures, especially when operating in areas such as the Persian Gulf. After being exposed to these temperatures for extended periods of time, on the range of hundreds of hours, aluminum will become sensitized. While this may seem like a long time, the service life of many ships can easily exceed 30 years or 262,800 hours. Stresses can come from a multitude of sources, such as structural loading from the weight of the ship, wave action as it interacts with the hull, residual stresses from welds, and stress concentrators from surface defects, damage or penetrations in the structure. All U.S. Navy ships operate in a salt water marine environment that is extremely corrosive; in fact, studies have been done that show that the spray from salt water is more corrosive than full immersion in water [5]. The interdependence of the three factors mentioned above is shown in the Venn diagram Figure 1.

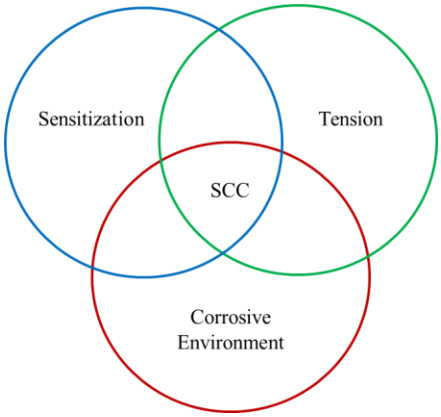

Figure 1. Venn Diagram Showing the Mutual Importance of Sensitization, Tensile Stress and Corrosive Environment on SCC

There are four basic stages to IGSCC: sensitization, pit nucleation, crack nucleation and crack growth (Figure 2). In the base, non-sensitized Al, the magnesium is in solution throughout the Al matrix. When the material is exposed to elevated temperatures for a prolonged period of time, the magnesium will diffuse out of solution and collect at the grain boundaries. At this point, the Al is considered to be sensitized; the more Mg that has diffused to the grain boundary, the more the sensitization level will increase. When subjected to a corrosive environment, localized corrosion consisting of pitting and intergranular corrosion (IGC) will occur. After stress has been applied for some period of time, cracks will nucleate at either the pits or from the IGC at the grain boundaries. While extensive studies have been done on the mechanisms of sensitization and crack growth in aluminum alloys [6-14], significantly less study has been done on pit nucleation, and especially crack nucleation [15-17]. This thesis will investigate the effects of tensile stress on the rates of sensitization, pit nucleation and crack nucleation.

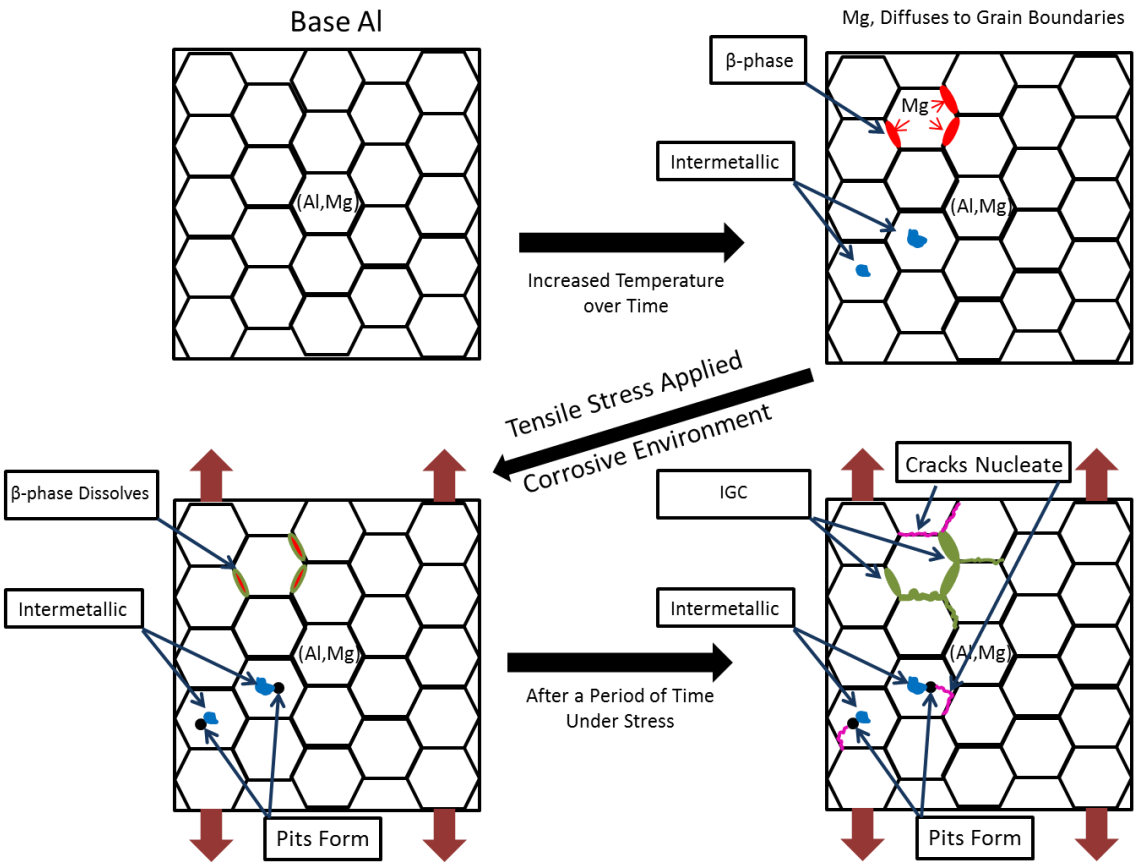

Figure 2. Schematic Showing the Process of Stress Corrosion Cracking

Work by Scully et al. showed the effects of time, sensitization and orientation on the rate of IGC of 5083 alloys [7]. They discovered that for a given degree of sensitization, the amount of corrosion increases as the length of exposure time to a corrosive environment is increased. Scully et al. found that significant IGC had occurred in as little as 24 hours when 5083 aluminum was exposed to a 0.6 M NaCl solution at a nitric acid mass loss test (NAMLT) value of 49 mg/cm^2 with an applied voltage of 0.73 V_{SCE}. They also showed that the amount of corrosion was a function of sensitization; higher mass loss values resulted in an increased amount of corrosion. During processing, 5083 aluminum is cold rolled, causing the microstructure to become anisotropic. The reference directions used in this thesis are:

- L, which is the longitudinal direction parallel to the length of the sample aligned with the rolling direction
- T, which is the long transverse direction parallel to the width of the sample and perpendicular to the rolling direction.
- S, which is the short transverse direction parallel to the thickness of the sample aligned orthogonal to the other two directions.

This system is used for sheet, extrusions, and forgings with nonsymmetrical grain flow [18]. All testing will be done on the LT plane with the samples oriented with the stress aligned with either the L or T directions (Figure 3). Scully et al. found that the ST plane with corrosion in the L direction was the most susceptible to IGSCC as measured by penetration depth per minute. However, the LT plane with corrosion in the T direction produced the most IGC leading to exfoliation (Figure 4).

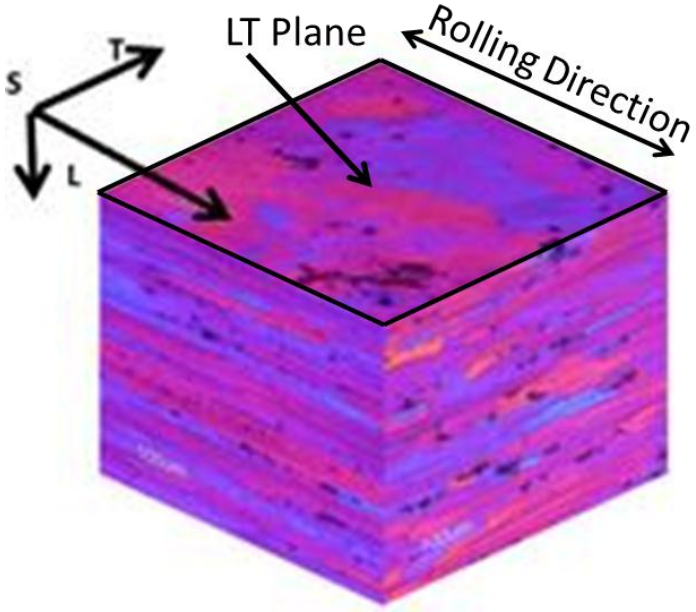

Figure 3. Orientation of L, T Directions and LT Plane with Respect to the Microstructure. From [7]

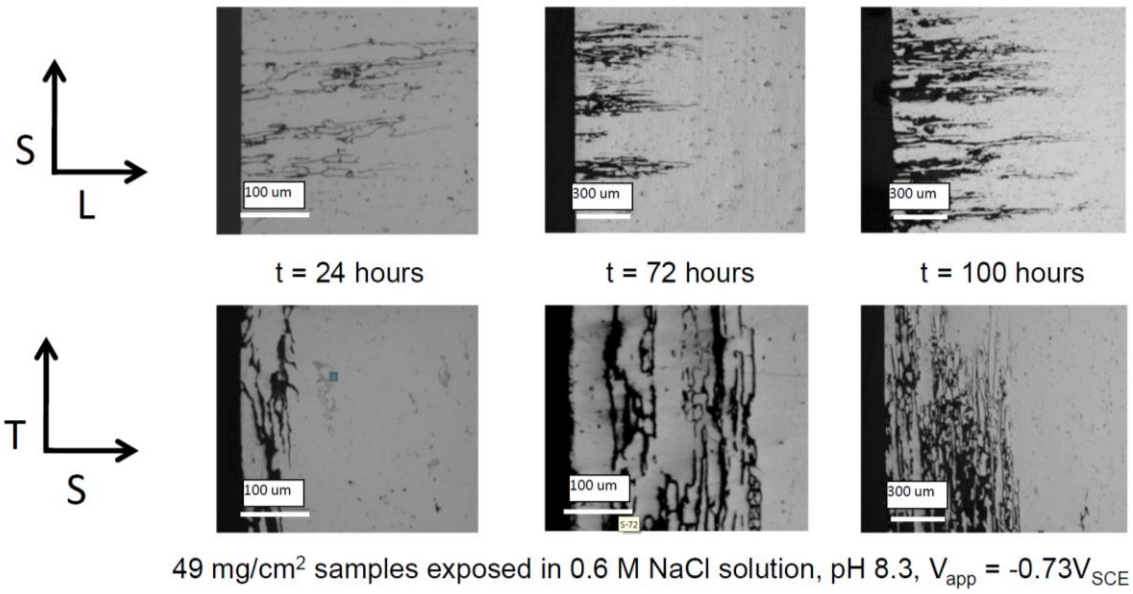

Figure 4. The Effects of Orientation on the Propagation of IGC Top image: IGC in the ST Plane in the L direction. Bottom Image: IGC in the LT Plane in the S direction. From [7]

1. Sensitization

In order for IGSCC to begin, the aluminum must become sensitized. The amount of sensitization depends upon temperature, length of time and orientation. The level of sensitization is based on how much magnesium has diffused out of solution to form grain boundary β-phase Al_3Mg_2. It should be noted that the formation of intragrain β-phase does not contribute to grain boundary sensitization. Since aluminum has a relatively low melting temperature (660°C), a high temperature is not needed for the diffusion of magnesium atoms to occur. As a result, aluminum can become sensitized when exposed to temperatures as low as 50°C, 323.15 K (that is, 35% of the melting temperature) for extended periods of time. As the temperature and length of time increases, more magnesium diffuses to the grain boundaries; as the deposits of β-phase grow, the aluminum becomes increasingly more sensitized. In order to determine the degree to which a piece of aluminum has been sensitized, a standard test was developed. The nitric acid mass loss test (NAMLT) ASTM G67 [19] is the standard test used by the Department of Defense for determining the degree of sensitization and the subsequent susceptibility for IGSCC. The test allows for a quantitative measurement of the degree of

sensitization that allows samples to be compared with each other. The weight of the sample is taken before and after the test. Since the nitric acid will preferentially attack the β-phase, the more β-phase present, the more material will be dissolved from the sample, decreasing its weight. This weight loss is then normalized with the surface area of the sample, thus giving a result in mg/cm^2. Once a sample has reached the level of 25 mg/cm^2, it is considered sufficiently sensitized to be susceptible to SCC [19]. The degree of sensitization that occurs in 5000 series aluminum is dependent on several factors, mainly temperature and time. Other factors, such as stress and orientation, will be examined in this thesis. As the temperature increases, so does the degree of sensitization. Also, the longer the exposure to elevated temperatures, the more the aluminum will become sensitized. Oguocha et al. determined that the degree of sensitization for a specified amount of time was the greatest at temperatures between 150°C and 200°C [4]. In Figure 5 shows a sensitization temperature vs. time and the mass loss per unit area.

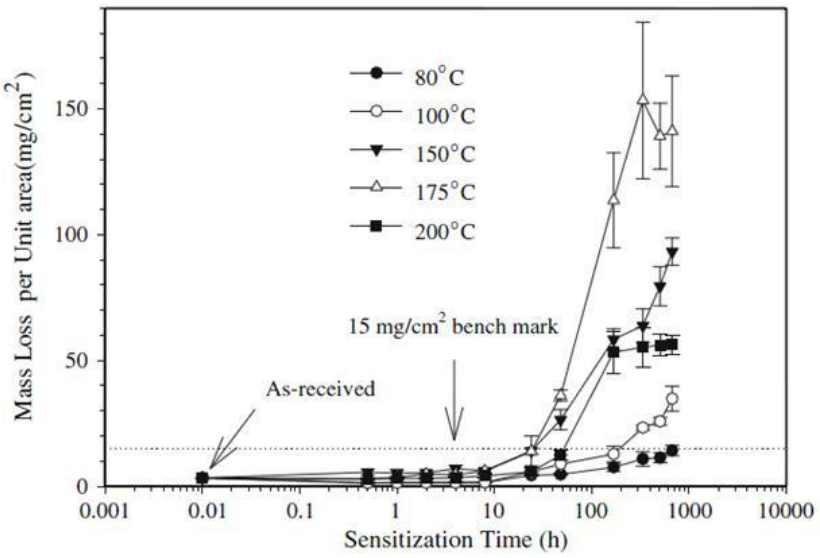

Figure 5. Effect of Sensitization Temperature and Time on IGC Susceptibility of AA5083-H116. From [4]

2. Localized Corrosion

Understanding localized corrosion is essential to the understanding of the starting mechanisms behind stress corrosion cracking. There are two distinct mechanisms behind localized corrosion in AA5xxx series alloys. One mechanism, through a process of

anodic dissolution of the aluminum matrix, results in the formation of circular pits around cathodic intermetallic particles, as listed in Table 1, a process generally referred to as "pitting." When the chloride ions present in sea water come in contact with aluminum, pitting nucleation will start, resulting in serious damage from corrosion mechanisms [15]. The corrosion attack is located around the Al_3Fe, and other cathodic, intermetallic particles, where there is a galvanic couple between the intermetallic and the aluminum matrix. This intermetallic phase is cathodic to the surrounding aluminum matrix [15]. Scully et al. also observed this cathodic reaction (a diagram of this process, which leads to pit formation, is shown in Figure 6). The basic anodic process in the corrosion of the aluminum is $Al \rightarrow Al^{3+} + 3e^-$. In addition to the galvanic couple, a process of hydrolysis takes place where the reduction of oxygen on intermetallic particles by the hydroxide ions in the solution causes a pH increase that in turn causes the dissolution of the oxide layer around the intermetallic particles and the matrix material. This process is represented by the equation $O_2 + 2H_2O + 4e^- \rightarrow 4OH^-$ [15]. Trueba et al. reported similar results for Mg-rich alloys such as 5083 where the iron-rich cathodic intermetallic particles were promoting the dissolution of the aluminum matrix [17]. Birbilis et al. studied the corrosion and pitting potentials for various intermetallics in all-aluminum alloy series, where they also found the β-phase, Al_3Mg_2, to be anodic to the surrounding aluminum; some of their data is summarized in Table 1 [20]. These studies have investigated the mechanisms behind the formation of pits in the aluminum matrix, but have not examined the possible influence of stress on the rate of pit nucleation.

The other localized corrosion process deals with the β-phase Al_3Mg_2 that is anodic to the surrounding matrix. The anodic dissolution of the β-phase allows for crack-like pit formation along the grain boundaries since the β-phase forms at the grain boundaries. This is known as intergranular corrosion (IGC). Oguocha et al. showed that the β-phase at the grain boundaries acts as a catalyst prompting crack growth and subsequent intergranular corrosion cracking through anodic dissolution [4]. As chloride ions exchange anions with hydroxide ions, the aluminum oxide layer, Al_2O_3, is broken down. The β-phase then begins to dissolve, forming crack-like pits as shown in Figure 7.

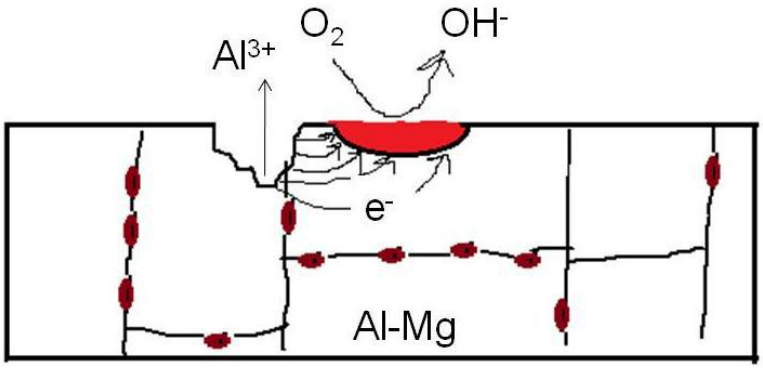

Figure 6. Showing the Cathodic Pit Formation and Cathodic Intermetallic Galvanic Couple. From [7]

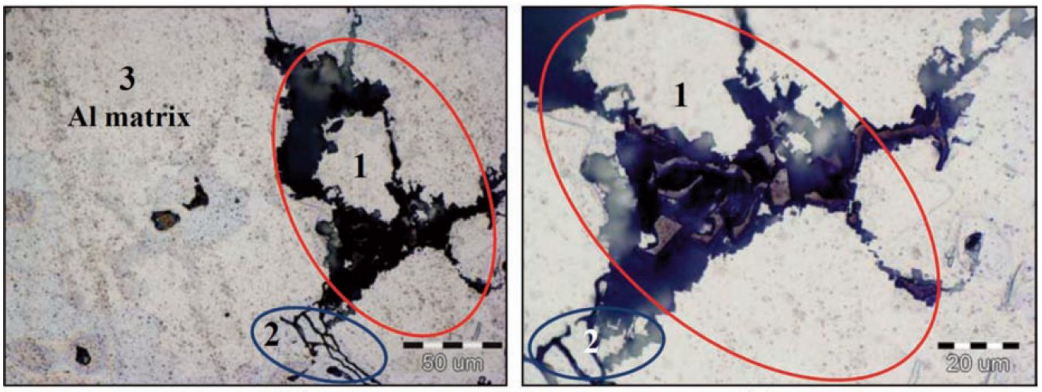

Figure 7. Red-Circled Area Showing Dissolved β-Phase Region. From [15]

Intermetallic	Corrosion Potential 0.6M mVsce	Cathodic/ Anodic Relative to Pure Al
Al	-849	
Al_3Mg_2	-1162	Anodic
Al_3Fe	-566	Cathodic
Mg_2Si	-1536	Anodic
$Al_{12}Mn_3Si$	-858	Anodic
Al_6Mn	-799	Cathodic

Table 1. Data Showing the Intermetallic that are Present in 5083 Aluminum, their Corrosion Potentials and if they are Cathodic/Anodic Relative to Al From [20]

3. Crack Nucleation

The mechanisms behind crack nucleation are the least understood of the four stages of IGSCC. An understanding of how cracks start will lead to a better understanding of how to prevent and predict their growth. The effects of stress on the process of crack nucleation have not been extensively investigated. Cracks nucleate in areas where a tensile stress is applied. In order for crack nucleation to occur, the material must be sensitized; this sensitization allows corrosion to occur. As the 5xxx series is most susceptible to IGC, this mode of corrosion is most likely responsible for the nucleation of cracks. As IGC progresses, the corrosion penetrates deeper into the surface, allowing the formation of crevice-like structures from which cracks can nucleate (Figure 8). One of the mechanisms described below will cause a crack to be nucleated. When a crack or flaw of critical size has been generated and a tensile stress is applied to the critically sized flaw, a crack will begin to grow.

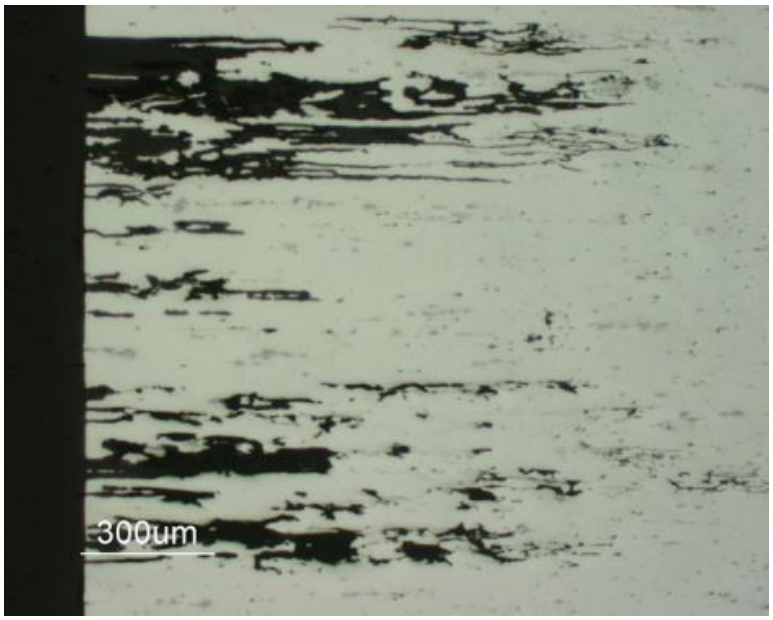

Figure 8. Showing the IGC in the L Direction after 100 Hours. From [7]

4. Crack Growth

The crack growth stage is the final stage, of SCC is the most widely studied and well understood stage. After the crack has been initiated through one of the processes discussed above, it will only grow when the applied stress intensity factor (K_1) is equal to or greater than the SCC resistance parameter (K_{1SCC}). K_{1SCC} is a material and environmentally-driven property that is not easily obtained. Work by Bovard, showed that increases in sensitization results in decreasing values for K_{1SCC} [5] (Figure 9). The value for K_1 is dependent on the stress applied as well as the length of the crack. As stress increases, so does the value for K_1. Also, if the stress level remains the same but the crack increases in length, the variable for K_1 will increase. There is a critical crack length at which, once reached, the crack will continue to grow until failure occurs. This length is given by the following equation:

$$a_{initiation} \geq \frac{1}{\pi}\left(\frac{K_{1SCC}}{(0.80*\sigma_{yield})\beta(a/W)}\right)^2 \qquad (1)$$

where,

$a_{initiation}$ = Critical Crack Length

K_{1scc} = Threshold Stress Intensity Factor, a Material Dependent Property

σ_{yield} = Yield Tensile Strength of the Material

β = Shape Factor Corresponding to the Crack and the Structural Component

a = Crack Length

W = Sample Width

The 5xxx series aluminum alloys are more susceptible to stress corrosion crack growth and subsequent failure in certain orientations. The manufacturing process of 5xxx series aluminum plate requires that the material be hot rolled. This process causes the material to be anisotropic; therefore, the material's properties are direction dependent. Work by Alcoa using uniaxial tensile testing found that applying stress along the different directions resulted in different rates of stress corrosion cracking and time to

failure. The stress applied in the L direction that is parallel to the rolling direction produced the longest time to failure, and thus the slowest rate of corrosion. When the stress was applied in the T direction that is perpendicular to the rolling direction, the time to failure was faster than the L direction, but slower than the final rolling direction the S. The S direction produced the fastest times to failure [8].

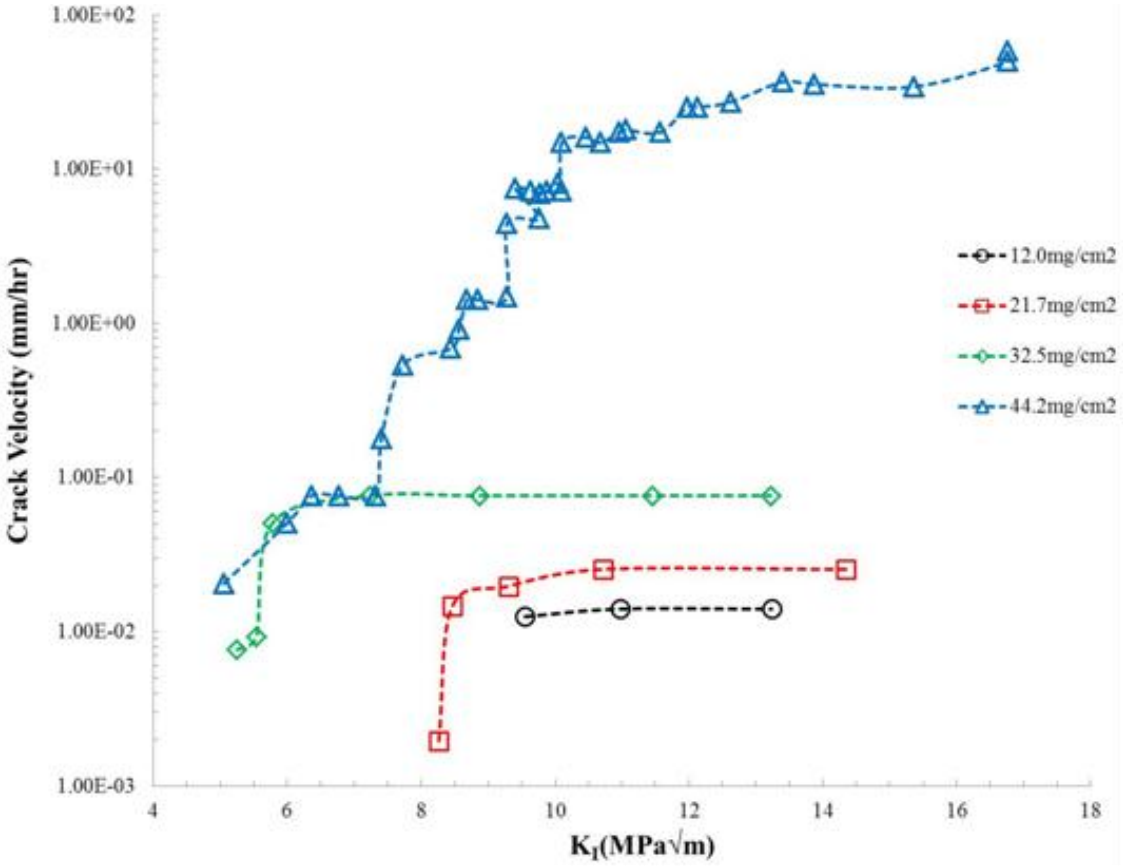

Figure 9. Increases in Mass Loss in ASTM G67 Correspond to Increases in S-L DCB Crack Growth Rates at Various Stress Intensity Factors. Data Converted to Metric Units. From [5]

Work by, Scully et al. and Bovard et al. came to the conclusion—that the ST plane is the most susceptible to SCC when looking at the rate of corrosion with an applied potential of 0.73 V_{SCE}. Testing on 5083 demonstrated that for NAMLT values between 32 to 44 mg/cm^2, 5083 samples fail in the shortest amount of time when tested

in the ST orientation, but do not fail in the LT orientation, even after extended exposure to a 3.5% NaCl solution. The rapid failures at low stress levels indicate that the value of K_{1SCC} in the ST orientation is low, suggesting that SCC susceptibility is strongly dependent on loading orientation [8].

While there is agreement that the preferential anodic dissolution of the β-phase, is central to SCC in AA5xxx alloys, there are several competing theories to describe the detailed mechanisms of the SCC. At the crack nucleation initiation point, hydroxides are formed due to the adsorption of Cl- ions from the NaCl in seawater on the surface layer. The eventual breakdown of the passive Al_2O_3 oxide layer and the dissolution of the aluminum substrate are enhanced due to the high concentration of Cl- ions in saltwater [10]. Three theories describe the mechanism of crack propagation in 5000 series aluminum alloys: propagation via the classic film ruptures model, environmental crack propagation by a mechanism involving hydrogen implement and crack propagation via corrosion tunneling. In the film ruptured model, the crack propagation is driven by increases in pH due to the chemistry of the oxide phase at the crack front. This model depends upon the repeated repassivation in order to keep the crack sharp for it to propagate. Figure 10 shows a graphical representation of this theory.

A second theory by Jones describes the crack propagation through hydrogen embrittlement according to the following steps:

- The preferential corrosion of the β-phase
- The conversion of the β-phase into Al_2O_3
- The generation of hydrogen during the corrosion of the β-phase
- The absorption of hydrogen ahead of the crack tip
- The growth of the crack due to hydrogen embrittlement

Since the β-phase is not continuous, the crack advances between the various particles through the hydrogen-induced process [21]. Figure 11 is a diagram of how this theory could produce crack propagation.

The third theory for the mechanism of crack propagation is corrosion tunneling. This theory is based on TGSCC that has not been shown to be a dominant cause for cracking in 5000 series alloys. Illustrated in Figure 12, this theory assumes that small corrosion tunnels are formed from the anodic dissolution of the β-phase. These tunnels grow in size until the remaining material between the tunnels is subjected to a tensile failure due to the applied stress [21].

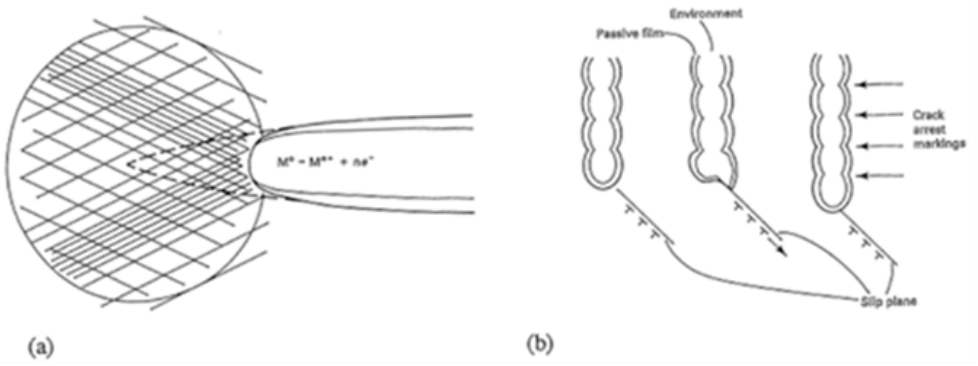

Figure 10. Representation of Crack Propagation by the Film-Rupture Model From [22]

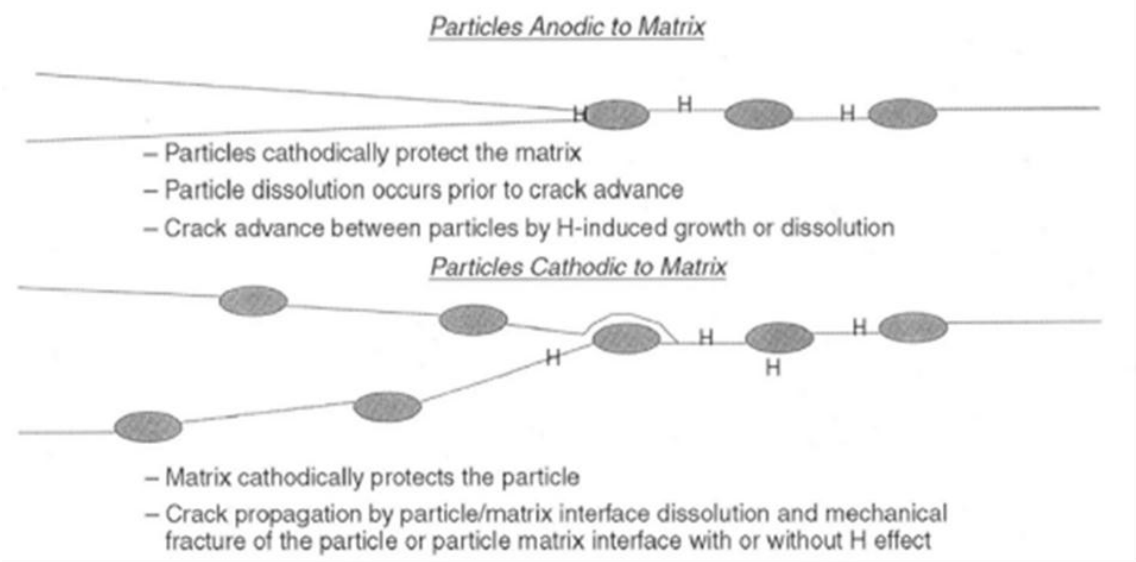

Figure 11. Diagram Showing Crack-Tip/Particle Interactions From [13]

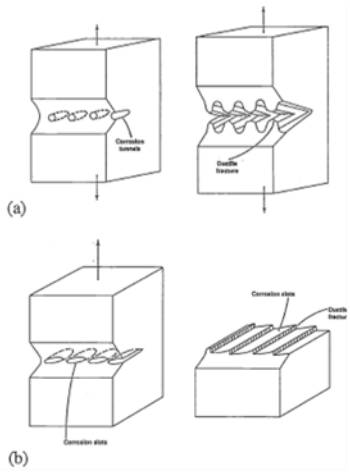

Figure 12. Illustration of Corrosion Tunnel Model (a) Schematic of Tunnel Model Showing the Initiation of a Crack by the Formation of Corrosion Tunnels at Slip Steps and Ductile Deformation and Fracture of the Remaining Ligaments (b) Schematic Diagram of the Tunnel Mechanism of SCC and Flat Slot Formation From [21]

C. OBJECTIVES

The effects of stress on the rates of corrosion are often overlooked, but their importance should not be underestimated. Research going back to the 1960s has examined the effects of applied stress and strain during corrosion. Green et al. studied the effect of plastic deformation on the corrosion rates of steel (strain accelerated corrosion) and found that plastic deformation increases the rate of corrosion when the steel is exposed to sulfuric and hydrochloric acids[23]. Green suggests that these effects are from an increase in the activity of surface sites for the dissolution process [23]. Despic et al. conducted similar research on steel as well as other metals, Mo, Ni and Cu. They found similar results for plastic deformation, but noted that in the elastic region, the overall effect was small [24]. A recent study by Krawiec et al., similar to the studies done on steel, was performed for 5052 aluminum. It revealed that an applied 5.5% plastic strain resulted in a highly heterogeneous strain field induced by the emergence of slip bands generated in the grains. The study also showed that the pitting potential was closely related to the strain field; areas with the highest density of slip bands produced the highest pitting potential [25].

While the results of these studies are interesting, they were dealing with a plastic region beyond yielding. Since most structures, including ship structures, are primarily designed to operate in the elastic region, the question of the effects of elastic stress on corrosion needs to be addressed. Liu et al. have done a few interesting studies addressing this question. One study looked at the influence of stress on the electrochemical noise on 7075 aluminum; it was found that an applied stress accelerated the formation of the electric double-layer at the alloy solution surface interface, and that as the stress was increased, the time for formation decreased [26]. A second, more interesting, study looked at the effect of hydrostatic pressure on the corrosion behavior of nickel. The results showed that as the pressure was increased, the probability of the formation and growth of larger pits increased. The stress localization effect had the greatest influence on the rate of pit growth. Liu et al. concluded that the localized corrosion resistance of nickel deteriorated in the presence of higher hydrostatic pressure [27]. These results suggest that stress could have an appreciable effect on the rate of IGSCC.

Determining the effect of stress on sensitization, localized corrosion, and crack nucleation will lead to a better understanding of how to predict where cracks will occur so that measures can be taken to mitigate their impact. For example, if a relationship between stress and the rate of sensitization can be determined, a finite element model of a loaded ship structure could be used to identify areas of increased stress and sensitization. As a result, preventative measures, such as locally reversing sensitization in 5000 series aluminum plate, could be taken in those areas [28]. The US Navy would save millions of dollar in repair costs as the problems with SCC could be averted before serious damage could occur. Therefore, the objectives of this thesis are to investigate the influence of stress on the first three stages of IGSCC: sensitization, pit nucleation and crack nucleation.

1. Design, Build and Implement an Apparatus for Performing a Four-point Bend Test

A four-point bending apparatus is needed because it will provide a constant maximum stress throughout the area between the inner supports. This is in comparison to a three-point bending apparatus that has been used previously where the stress varies

along the entire length of the sample and is at maximum at the center. With a four-point bending apparatus, a sample can be subjected to a uniform tensile stress in order to test the effects of stress on various components of the SCC problem. The horizontal geometry will allow for the exposure of the surface under tension to salt water during testing.

2. Determine the Effect of Stress on the Rate of Sensitization of 5083 Aluminum Alloy

Sensitization is the first step in the process of SCC. Aluminum will sensitize when in the presence of elevated temperatures for extended periods of time. This objective will determine if applying a tensile, elastic stress during elevated temperature exposure will affect the rate and degree of sensitization. The amount of sensitization will be compared with different levels of stress.

3. Determine the Effect of Stress on the Rate of Localized Corrosion of 5083 Aluminum Alloy

Using the four-point bending apparatus, this objective will determine if the rate localized corrosion, both pitting and IGC, on the surface of an aluminum sample will be affected by an applied tensile stress. The relationship between the formations of pits while being subjected to an applied stress has not been investigated. The pitting will be characterized by the type of localized corrosion, the size of individual pits, and the density at which they occur. We will also investigate the role of plate orientation in this process.

4. Test the Effect of Stress on the Rate of Crack Nucleation in 5083 Aluminum Alloy

This objective will utilize the four-point bending apparatus to test if the rate of crack nucleation is affected by the level of tensile stress on the surface. Crack nucleation is part of the process that leads to long crack growth and ultimately failure; the effect of stress on this particular process is not well known. Also questioned is at what stress level a crack will nucleate. It is known that a tensile stress is needed for a crack to nucleate, but at what amount of stress this will occur has not been closely studied.

II. EXPERIMENTAL METHODS

A. FOUR-POINT BENDING APPARATUS

1. Fabrication and Testing of Bending Apparatus

The design of the apparatus was based on the diagram for a four-point bending test in the ASTM G39 that is shown in Figure 13. Section 10.4 of ASTM G39 specifies that the specimen shall be a flat strip 25.4 mm (1 in.) to 50.8 mm (2 in.) wide and 127 mm (5 in.) to 254 mm (10 in.) long [29]. Therefore, the bending apparatus was designed to accommodate a sample that was 25.4 mm (2 in.) wide and 139.7 mm (5.5 in.) long. It also specifies that the inner supports shall be located symmetrically around the midpoint between the outer supports [29]. The four-point bending apparatus was made from 316 stainless-steel. Stainless steel is corrosion resistant and has a significantly higher elastic modulus as well as a much high melting temperature than the aluminum; therefore, the stainless steels compliance will be significantly less than that for the aluminum samples. The apparatus was designed using solid works to have four points of contact on the sample in accordance with the ASTM G39. The channel running down either side was sufficiently wide that the end of the sample could rotate freely, allowing it to be modeled as a simply supported beam. The apparatus was designed as a constant displacement test; #10 stainless steel screws with 32 threads per inch where used to displace the samples. A schematic from Solid Works is shown in Figures 14 and 15 and the completed apparatus is shown in Figures 16 and 17.

The equation used to calculate the stress at the mid-portion of the sample is equation 6 from the ASTM handbook [29]:

$$\sigma = \frac{12Ety}{(3H^2 - 4A^2)} \qquad (2)$$

where,

- σ = Maximum Tensile Stress (Between Inner Supports)
- E = Modulus of Elasticity of the Sample
- t = Thickness of Sample

- y = Maximum Deflection (Between Outer Supports)
- H = Distance Between Outer Supports
- A = Distance Between Inner and Outer Supports

The following constant values where used in the stress calculations.

- E = 70326.54 MPa (1.02E7 psi)
- t = 6.35 mm (0.25 in)
- H = 132.97 mm (5.235 in)

Since this is a displacement-controlled test, the amount of displacement can be related to the number of screw turns. By multiplying the amount the screw is turned by $\frac{1}{TPI}$ where TPI is the threads per inch of the screw, 32 TPI screws where used. It is assumed that the screw displacement equals the maximum deflection (y) in the above calculation. Because of this, the maximum deflection at the midpoint was measured with a micrometer in all the experiments. The above relationship is based on small deflections where the value of y/H is less than 0.1 [8]. Using the above equations and constant values, Table 2, which gives the stress and strain values associated with the amount of screw turns or midpoint displacement, was calculated. The values for strain were calculated from the stress values using: σ/E.

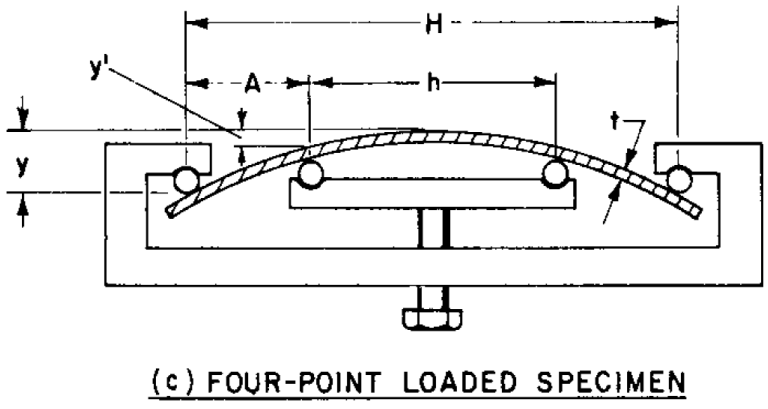

Figure 13. Four-point Diagram from ASTM G39 From [29]

Screw Turns	Displacement In	Stress Psi	Strain	Stress MPa	y/H < 0.1
0.1	0.003125	1367	0.000134	9	0.00060
0.2	0.00625	2733	0.000268	19	0.00119
0.3	0.009375	4100	0.000402	28	0.00179
0.4	0.0125	5467	0.000536	38	0.00239
0.5	0.015625	6834	0.00067	47	0.00298
0.6	0.01875	8200	0.000804	57	0.00358
0.7	0.021875	9567	0.000938	66	0.00418
0.8	0.025	10934	0.001072	75	0.00478
0.9	0.028125	12301	0.0012059	85	0.00537
1	0.03125	13667	0.0013399	94	0.00597
1.1	0.034375	15034	0.0014739	104	0.00657
1.2	0.0375	16401	0.0016079	113	0.00716
1.3	0.040625	17768	0.0017419	123	0.00776
1.4	0.04375	19134	0.0018759	132	0.00836
1.5	0.046875	20501	0.0020099	141	0.00895
1.6	0.05	21868	0.0021439	151	0.00955
1.7	0.053125	23235	0.0022779	160	0.01015
1.8	0.05625	24601	0.0024119	170	0.01074
1.9	0.059375	25968	0.0025459	179	0.01134
2	0.0625	27335	0.0026799	188	0.01194
2.1	0.065625	28702	0.0028139	198	0.01254
2.2	0.06875	30068	0.0029479	207	0.01313
2.3	0.071875	31435	0.0030819	217	0.01373
2.4	0.075	32802	0.0032159	226	0.01433
2.5	0.078125	34169	0.0033499	236	0.01492

Table 2. Stress-Strain Calculations Based on Displacement or Screw Turns, The Yellow Bar Designates the approximate yielding Point

To verify that the above table correctly predicted the stress at the midpoint of the samples, strain gauges were attached to two different samples. The samples were displaced and the calculated strain value was compared to the measured value given by the strain gauges. The equipment consisted of 350 ohm Omega quarter bridge linear strain gauges were attached to a National Instruments NI-CDAQ-9174 data acquisition

module that was connected to a computer running Lab View Express. The samples were displaced by increasing amounts, after which the values of strain were compared. The calculated values were found to match the strain gauges values, verifying that the stress values calculated by the ASTM equation where correct.

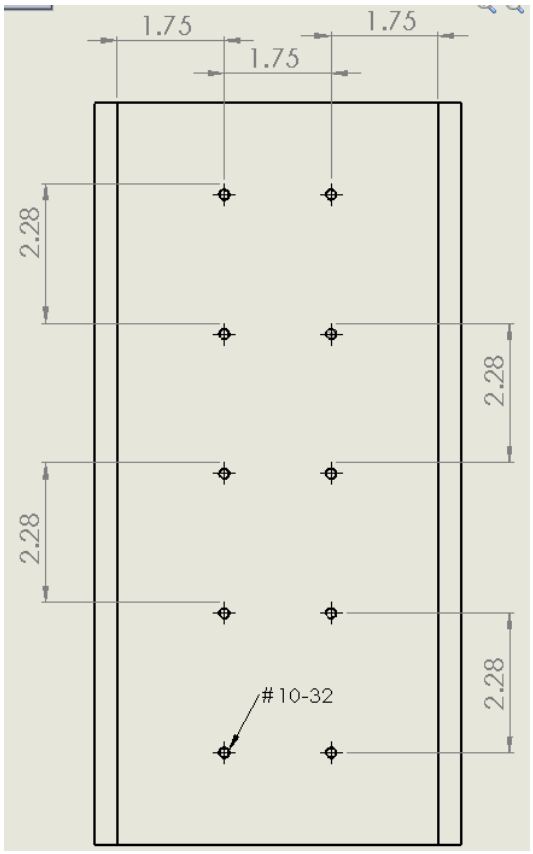

Figure 14. Solid Works Schematic Showing a Top View

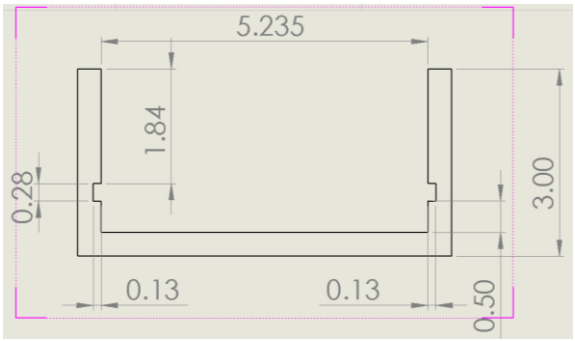

Figure 15. Solid Works Schematic Showing a Front View

Figure 16. Top View of Four-Point Bending Apparatus with Samples Loaded

Figure 17. Front View of Four-Point Bending Apparatus with Samples Loaded

2. Fabrication of Test Samples

For this thesis, the material used for all the samples in the following tests is the aluminum alloy AA5083 with a H116 heat treatment. The material composition is

magnesium 4.7, manganese 0.9, iron 0.20, silicon 0.10, chromium 0.08, zinc 0.03, copper 0.03 and titanium 0.01. The composition was certified by the American Bureau of Shipping. The aluminum was in plate form, 6.35 mm (0.25 in) thick. Samples of the size 139.7 mm (5.5 in) x 50.8 (2.0 in) where machined from the plate. This sample size was used in all bending tests. Two types of samples where cut, one with the long axis of the sample parallel to the rolling direction (L) and one with the long axis perpendicular to the rolling direction (T) (Figure 18).

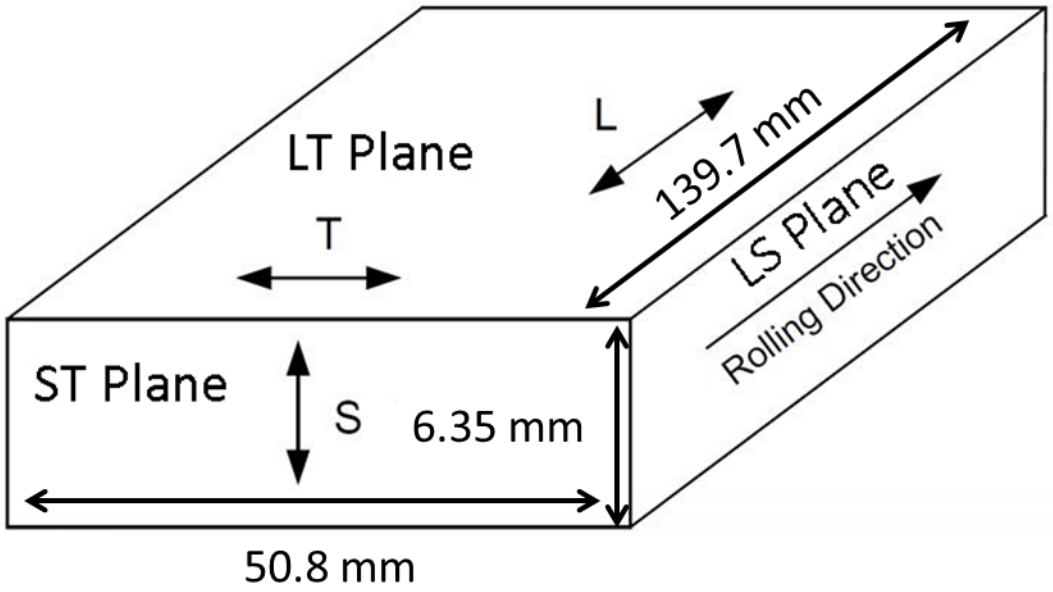

Figure 18. Direction of Applied Stress vs. Rolling Direction and Sample Dimensions for the L Sample

B. RATE OF SENSITIZATION EXPERIMENTS

1. NAMLT

Samples for the NAMLT were sensitized using two different conditions: 175°C for 100 hours and 80°C for 50 hours. For both conditions, an MTI gravity convection oven was used to heat the samples for the required amount of time (Figure 19). For the remainder of this thesis, the time component of the sensitization conditions will be omitted since the same temperature and time combination was used for all tests. The oven was preheated to the required temperature before the samples were placed in it. Once the

length of time had expired, the samples were taken out and placed on the counter until they cooled to room temperature.

Figure 19. Gravity Convection Oven Used to Sensitize Samples

The samples were heated in the oven while under an applied stress using the four-point bending apparatus. In order to set the stress level, the midpoint displacement was measured using a micrometer. The original design for the four-point apparatus needed to be shortened to fit into the oven. An attempt to use the full size apparatus in a larger furnace was abandoned because the temperatures being used proved to be problematic to control. The following range of stress levels were used L from -200 to 200 MPa and T from -200 to 200 MPa, the specific values are listed in Table 8 in the appendix.

The sensitized samples were sectioned into test specimens using a Struers Secotom-10 high speed saw with a 50A20 cutoff wheel. An inch-wide strip was marked in the center of each sample and cut creating 50.8 x 25.4 x 6.35 mm (2 x 1 x 0.25 inch) samples. The samples were cut along the short side to make two identical 25.4 x 25.4 x 6.35 mm (1 x 1 x 0.25) inch specimens. Since one side of these samples was in tension

and one side in compression, the samples were cut along the thickness to make separate tension and compression samples. Therefore, each 50.8 x 25.4 x 6.35 mm (2 x 1 x 0.25 inch) sample made four test specimens, two identical tensions and two compressions.

A 3.175 mm (1/8-inch) hole was drilled into the top of each specimen. This was to allow the specimen to be hung on a rack over the beaker of acid. Since the NAMLT attacks the surface of the specimen, the specimens must be suspended so that the acid can have access to all sides. Dimensions of the specimens were measured using a micrometer. This procedure was necessary since the cutting process was not precise; therefore, the size of the specimens would vary slightly. Once the dimensions were determined, the surface area was calculated using the following formula (Figure 20):

$$A_H = 2\pi \frac{1}{16}\left(\frac{(T_1 + T_2)}{2}\right) \tag{3}$$

$$SA = 2LW + 2\left(\frac{(T_1 + T_2)}{2}\right)L + LT_2 + WT_1 + A_H - 2\pi\left(\frac{1}{16}\right)^2 \tag{4}$$

where,

L = Length of the Sample

W = Width of the Sample

T_1 = Thickness of the Sample

T_2 = Thickness of the Sample

SA = Surface Area of the Sample

A_H = Area Added by Drilling a Hole

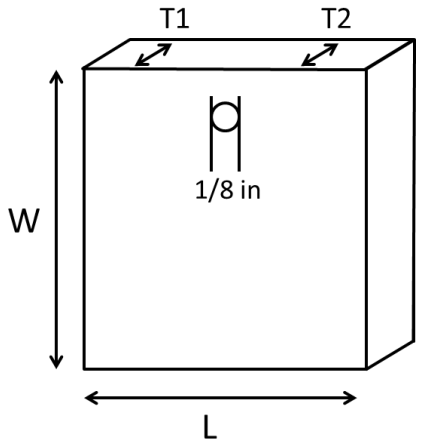

Figure 20. Diagram of Sample Geometry for NAMLT Samples.

The NAMLT was conducted in accordance with ASTM G67 [19]. The samples were etched using solutions of reagent grade sodium hydroxide and 70% nitric acid. The solutions were heated on hot plates to temperatures of 80°C and 30°C respectively. The specimens were first placed into the sodium hydroxide for 60 seconds, then rinsed with distilled water and placed in the nitric acid for 30 seconds, then rinsed a second time with distilled water. The specimens were weighed using a Sartorious CP225D scale and the weight recorded in grams on a spreadsheet. The specimens were hung from the rack using 18-gauge bell wire because it was sufficiently resistant to the nitric acid. Care was taken to arrange the specimens so that no two samples were in contact with each other or the sides of the beaker. The surface area of the specimen was multiplied by three to determine the amount of acid needed in accordance with the ASTM G67; the total for all specimens being tested equaled the amount in milliliters of acid required. In order to reduce the possibility for error, multiple specimens were tested at the same time. To facilitate the testing, a 2-liter beaker was used to contain the acid and the specimens. To heat the acid in the beaker to the required 30°C, the beaker was placed in a 10-gallon aquarium that was filled with approximately three gallons of distilled water. Fig. 20 shows the test setup. A 100 Watt Aqueon submersible aquarium heater was used to keep the water at the required 30°C for the duration of the test. Such a large volume of water was needed in order to provide thermal stability since the test was extremely sensitive to small changes in the temperature of the acid. Before the specimens were placed in the acid, the water in the aquarium and the beaker containing the acid were allowed to sit for 24 hours so that thermal equilibrium could be reached. The specimens were placed in the acid for 24 hours, then removed and rinsed with distilled water while being scrubbed with a brush. The specimens were allowed to air dry and their weights were recorded using the scale previously mentioned. The sensitization level was calculated by subtracting the final weight from the initial weight divided by the surface area of each specimen.

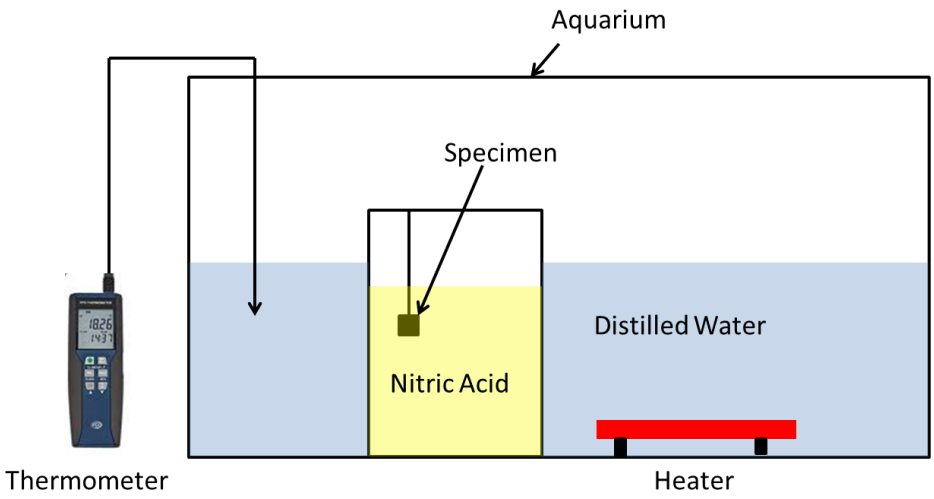

Figure 21. Samples Being Tested in NAMLT

2. Rockwell Hardness

Hardness tests were completed on the samples to measure the different levels of sensitization. The measurements were made using a Wilson Rockwell hardness tester. A Rockwell B hardness scale with a 100 kg load using a 16 mm diameter steel ball for the indenter was used. There are three indentations taken for each sample; the results of which were averaged for a final hardness value.

3. Optical Microscopy

Optical microscopy was used to determine the amount of β-phase present in five different samples. The selected samples where sensitized using the procedure previously mentioned with the following conditions: 80°C for 50 hours and 175°C for 100 hours. Table 3 summarizes the samples tested.

Sample	Stress Level	Orientation	Sensitization Condition
6	0	L	None
27	0	T	80°C for 50
64	0	T	80°C for 50
63	28	T	175°C for 100
32	28	T	175°C for 100

Table 3. Sensitization Microscopy Samples and Conditions

The samples were cut into small sections using the Struers Secotom-10 high speed saw. Each sample was mounted into a Buehler red phenolic premold for ease of polishing. A Buehler Simplimet 2 was used to mount the samples in the premolds. The steps used to polish the samples were as follows:

- Sanded using 600 grit silicon carbide paper
- Sanded using 1200 grit silicon carbide paper
- Sanded using 2400 grit silicon carbide paper
- Polished using Buehler Metadi monocrystalline diamond 1μ oil-based suspension with water as a lubricant to keep the sample surface cool
- Polished using Buehler Mastermet colloidal silica solution in a Vibromet 2 vibrating polisher for a period of five hours

The surface of the sample was etched with a solution of 40% phosphoric acid at 35°C for three minutes. The amount of β-phase on each sample was characterized by taking images using the Nikon Epiphot 200 optical microscope at different fields of view using magnifications of 25 X, 100 X, 200 X, 500 X and 1000 X.

C. PITTING NUCLEATION TEST

Three samples were used in the pitting nucleation test. The samples were sensitized utilizing the MTI gravity convection oven with the following condition: 175°C for 100 hours. The samples were sensitized with no applied stress. The test used the four-point bending apparatus to apply a tensile stress to the surface of the now sensitized samples. The sample conditions tested are shown in Table 4 as follows:

Sample	Stress Level (MPa)	Orientation
12	100	L
40	100	T
2	0	L

Table 4. Pitting Nucleation Test Conditions

A highly polished sample was required so that the formation of pits or corrosion could be clearly seen. The polished surface gave a starting point to compare the exposed samples to. As the samples were too large for the sample holders, in order to use the Buehler Automet 2 the samples were taped to the bottom of the sample holder using

double sided scotch extreme mounting tape (Figure 22). The samples went through the following metallographic preparation procedure:

- Sanded using 320 grit silicon carbide paper, Buehler Automet 2 settings. Speed: 150 RPM. Force: 30 lbs. Time: 15 minutes. Lubricant and coolant: water. Then rinsed with distilled water.
- Sanded using 600 grit silicon carbide paper, Buehler Automet 2 settings. Speed: 150 RPM. Force: 30 lbs. Time: 15 minutes. Lubricant and coolant: water. Then rinsed with distilled water.
- Sanded using 1200 grit silicon carbide paper, Buehler Automet 2 settings. Speed: 150 RPM. Force: 30 lbs. Time: 15 minutes. Lubricant and coolant: water. Then rinsed with distilled water.
- Sanded using 2400 grit silicon carbide paper, Buehler Automet 2 settings. Speed: 150 RPM. Force: 30 lbs. Time: 15 minutes. Lubricant and coolant: water. Then rinsed with distilled water.
- Polished using black foam pad with Buehler Metadi monocrystalline diamond 3 µ oil-based suspension, Buehler Automet 2 settings speed: 300 RPM force: 15 lbs., time: 15 minutes, lubricant: water, then rinsed with distilled water.
- Polished using black foam pad with Buehler Metadi moncrystalline diamond 1 µ oil-based suspension, Buehler Automet 2 settings. Speed: 300 RPM. Force: 15 lbs. Time: 30 minutes. Lubricant: water. Then rinsed with distilled water.

Figure 22. Image Showing Mounting Arraignment for Polishing Samples with the Automet

So that a progression of the formation of pit nucleation could be captured, a grid was laid out on the surface of the sample so that images could be taken at exactly the same locations each time. A 24 x 24 mm grid was placed on the surface using a HVS-1000 Digital Microhardness tester using a Vickers indenter with indents spaced every 2 mm. The samples were loaded into the four-point bending apparatus and displaced to the specified amount. The samples were placed in direct sunlight and a 1.25 ml spray of 3.5 weight percent (wt%) sodium chloride solution was applied to the samples every hour. The test was run in increments of 2, 4, 8, 16, 32 and 64 hours. After each test segment, the samples were removed from the apparatus and washed with distilled water and

methanol. A series of micrographs was taken at the four corners of the grid for each sample. Four images were taken at each location on each sample at the following magnifications: 25 X, 100 X, 200 X, and 500 X for a total of 16 images per sample.

A simple statistical approach was taken to determine the amount of localized corrosion on each of the samples. An area consisting of twenty-five 2 x 2 mm boxes was observed (Figure 23). Each box was examined for the presence of either pitting or IGC. If any localized corrosion was present, the box was counted. The total number of boxes containing pitting or IGC was totaled for each sample. The total localized corrosion was the sum of the totals for pitting and IGC. These values were represented by X/25, where X is the number of boxes containing corrosion. Note that some of the boxes contained both IGC and pitting. Therefore, the total localized corrosion is less than the sum of the pitting and IGC totals. This metric was performed after exposures of 32 and 64 hours.

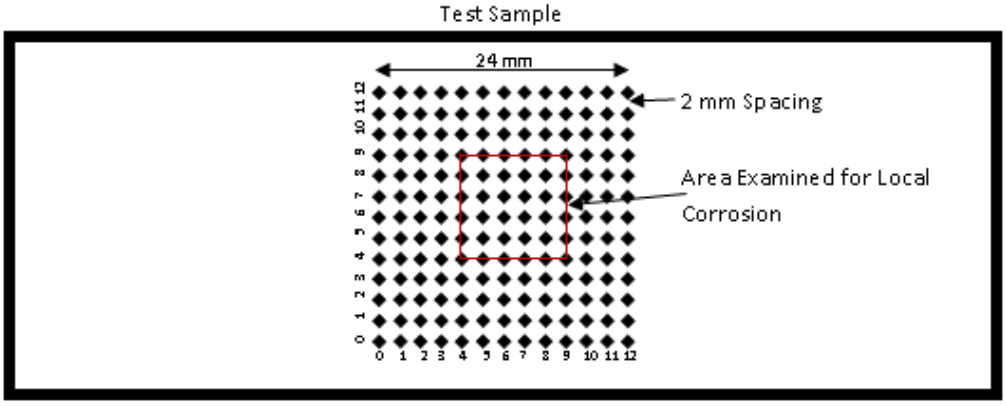

Figure 23. Diagram Showing the Layout and Orientation of the Grid on the Sample, the Red Box Denotes the Area Examined for Statistical Analysis

D. CRACK NUCLEATION TEST

The four-point bending apparatus discussed above was used to perform this test. Five samples were placed in the apparatus. Each sample was sensitized with no applied stress using the gravity convection oven at 175°C for 100 hours. The samples tested and the conditions for each sample are shown in Table 5. The samples were loaded into the four-point apparatus and displaced to the specified level. Two separate tests were conducted on the samples. One was a controlled indoor laboratory test, the other an

outside test where the samples were exposed to the elements. A solution of 3.5 wt% sodium chloride with 0.03 wt% hydrogen peroxide was used for both tests.

Sample	Stress Level (MPa)	Orientation
19	151	L
20	0	L
15	0	L
22	0	T
21	151	T

Table 5. Crack Nucleation Test Sample Conditions

1. Laboratory Test

With the samples in the four-point apparatus, the midpoint displacement was measured and set to 0.05 inches for a stress of 151 MPa. The solution was applied with a dropper; several drops were put onto the center of each sample at intervals of approximately 12 hours. The test was conducted in this configuration for a period of four weeks; after that the test was stopped and the samples were cleaned with distilled water. Photographs of the samples were taken with a camera. Because of the pre-existing surface conditions, it was difficult to determine what changes had occurred to the samples. Therefore, the samples were cleaned and polished using the previously mentioned metallographic preparation procedure described in section C. The samples are placed back into the four-point bending apparatus with the testing conditions remaining the same as before. To apply the sodium chloride solution to the samples, the drip system was constructed that allowed the same amount of solution to be dripped on each sample. The solution was dripped on the samples approximately every eight hours. A line of silicone was placed across the top and bottom of the sample so that the solution would not run off the edges because of the curvature of the sample. The dripping portion of the test was run for a period of four weeks. After completion of the dripping test, the results were recorded by taking photographs of each of the samples.

The last laboratory exposure method used a spray bottle to mist the solution onto each sample. A fine mist of solution was applied to each sample at intervals of twelve

hours; this portion of the test was conducted for a period of six weeks. After completion, the apparatus and samples were moved for the outdoor phase of testing.

2. Outdoors Testing

The test was moved outside and positioned so the samples were directly exposed to UV radiation and the elements. The samples remained in the four-point apparatus loaded to the same conditions as in Table 5. The samples were kept outside 24 hours a day for the entirety of the test. During this test, the application of solution by spray bottle every 12 hours for two weeks was continued, and the solution remained the same. After the two-week period had elapsed, a final element was added to the test. A section of the sample was outlined with silicone around all four sides so that it was watertight. Iron filings were added to the inside of this area, which was filled with a solution applied with the spray bottle. The samples remained outside continuously and the sectioned off area was filled with solution approximately every 12 hours. This portion of the test was allowed to run for four weeks. After completion of the outdoors testing, the samples were removed from the apparatus and the surface of the samples was cleaned with distilled water and methanol. The final results of the test were recorded by taking photographs of each sample. A series of optical microscopy images was also taken in order to look for any cracks that may have been too small to see by visual inspection alone.

III. RESULTS

A. FOUR-POINT BENDING TEST

Results from strain gauge testing show that stress and strain varied linearly with displacement. Using equation 1, calculated stress values were obtained. Using Young's modulus, these stress values where changed to values of strain. When the calculated strain values are plotted against the strain values obtained from experimental testing using strain gauges, the values match closely (Figure 24, 26). Depending on the source, values for the yield stress for 5083-H116 aluminum range from 214 to 228 MPa. Therefore, strain values to 90 to 95% of yield were tested with the strain gauges. In bending, the stress is not uniform throughout the section because the top half is in tension while the bottom is in compression. The maximum stress occurs at the outside surfaces. Therefore, yielding does not occur inside the section unless yielding occurs at the outside surfaces.

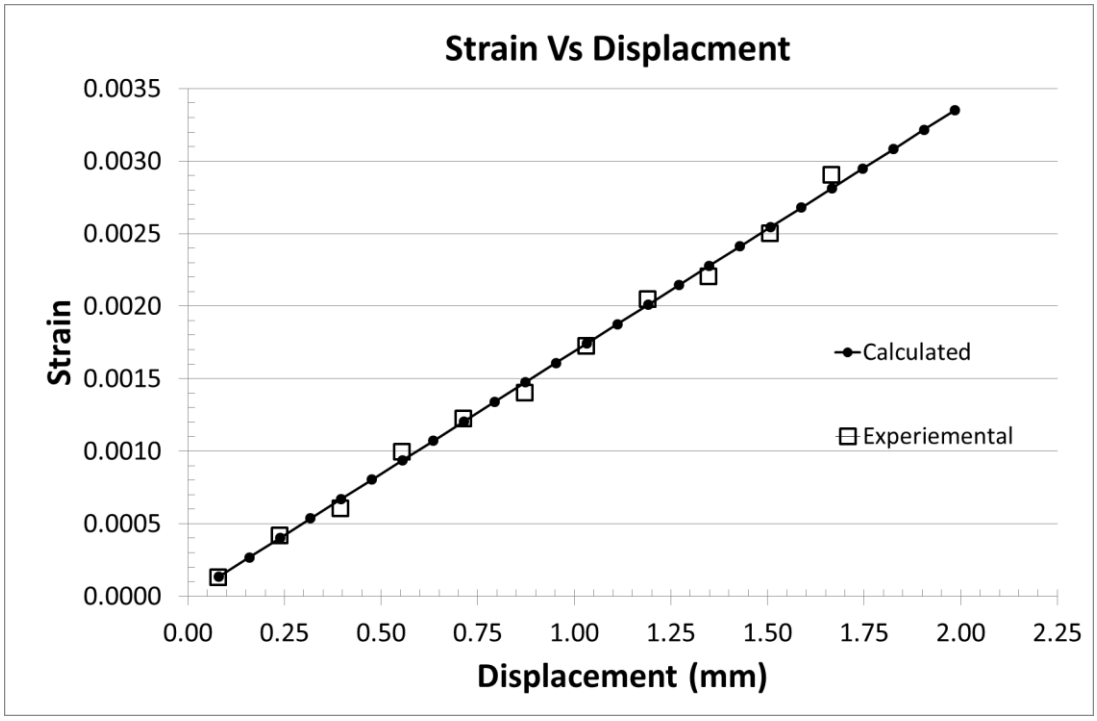

Figure 24. Data for Calculated and Experimental Values for Strain Vs. Displacement

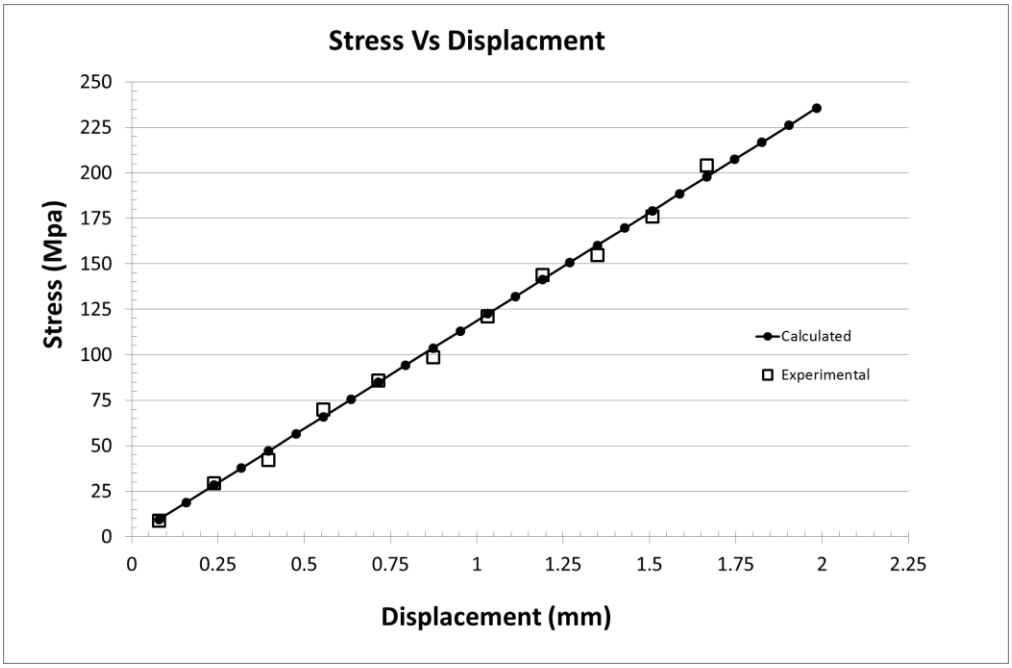

Figure 25. Data for Calculated and Experimental Values for Stress Vs. Displacement

B. SENSITIZATION EXPERIMENTS

1. Nitric Acid Mass Loss Testing (NAMLT)

NAMLT data for the 175°C condition shows no clear relationship between stress and sensitization level. The data for samples sensitized at 175°C suggests that any level of applied stress, whether tensile or compressive, will lower the sensitization level compared to the unstressed samples (Figure 26). At the 175°C sensitization condition, Oguocha et al. measured a NAMLT value of 120 mg/cm^2; the current 175°C NAMLT data showed roughly half of that value (Figure 26). However, the NAMLT data for the 80°C test condition at the 9 MPa level suggested that small levels of stress, whether tensile or compressive, increased the amount of sensitization. This effect seemed to diminish at the higher stress levels (Figure 27). At stress levels above 9 MPa, the mass loss seems to decrease down to levels below that for the stress-free control. Each test condition had two measurements. The error bars were derived from the precision in mass, length, and surface area measurements. The scatter in the NAMLT data may be too great to draw any strong conclusions from this set of tests (Figures 26, 27).

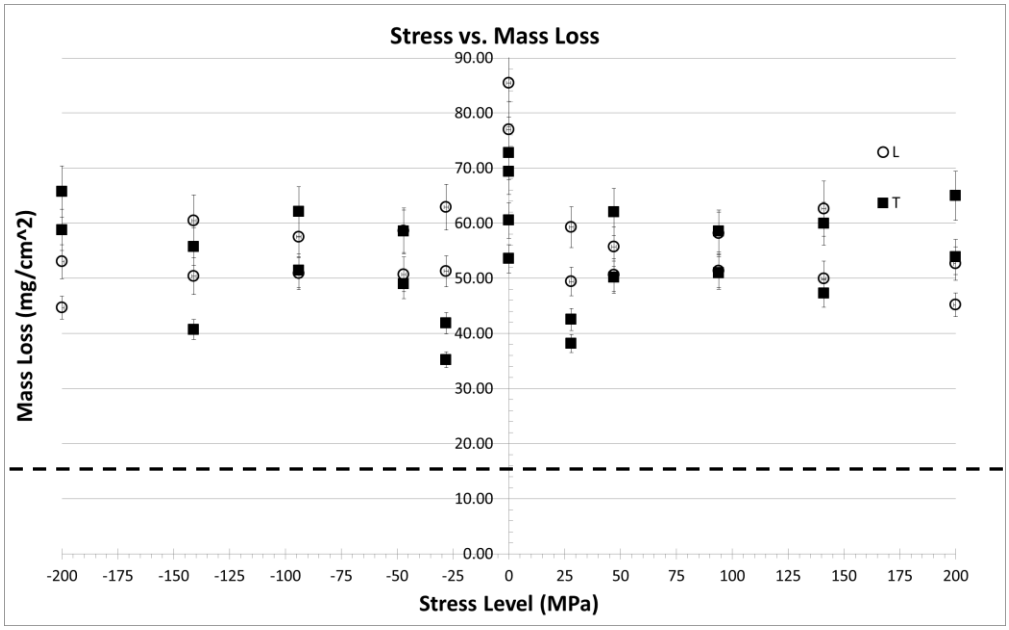

Figure 26. Data for Sensitization Level Vs. Stress, 175°C for 100 Hours, Dashed Line Represents Level at Which the Material is Considered Sensitized

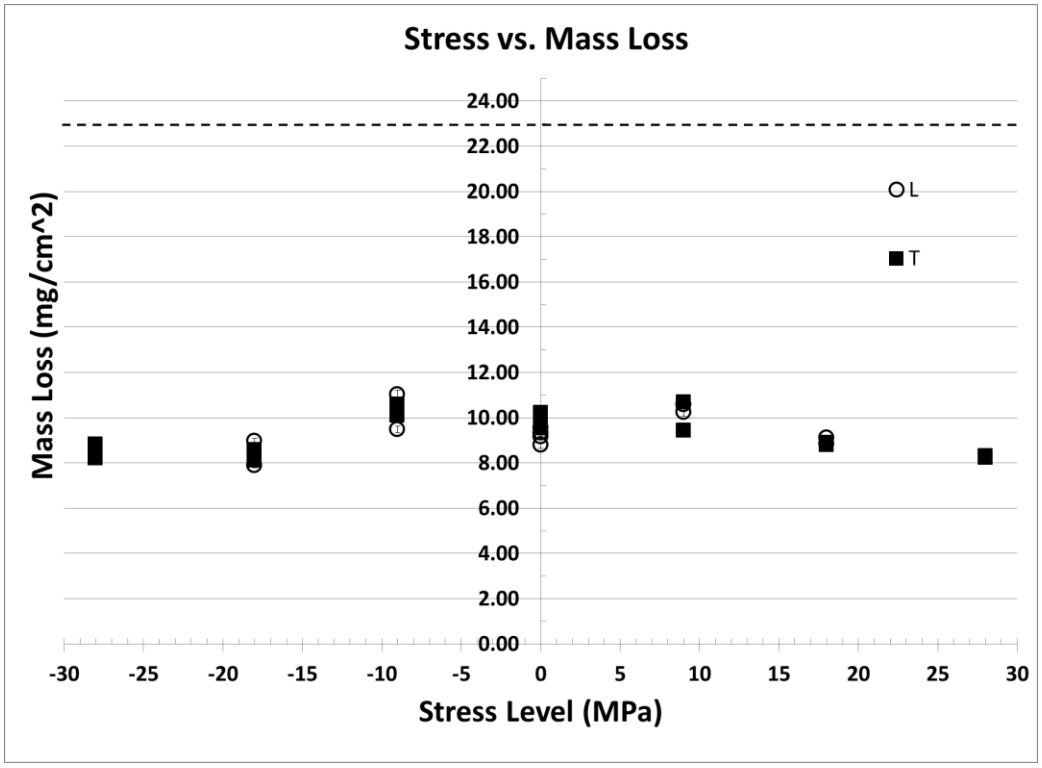

Figure 27. Data for Sensitization Level Vs. Stress, 80°C for 50 Hours, Dashed Line Represents Level at Which the Material is Considered Sensitized

2. Hardness Tests

Hardness testing showed no clear relationship between stress during sensitization and the resultant hardness level. For the samples sensitized at 175C, there was no clear trend that would show that stress has any effect on the hardness values of the samples. The data does suggest that the sample direction during sensitization matters. The L samples sensitized at 175°C were systematically harder than those sensitized under stress in the T direction. This direction dependence was not observed for the 80°C samples tested. The 80°C samples have hardness values similar to those of the 175°C samples. All sensitized samples had hardness values less than the as-received non-sensitized sample (Figure 28).

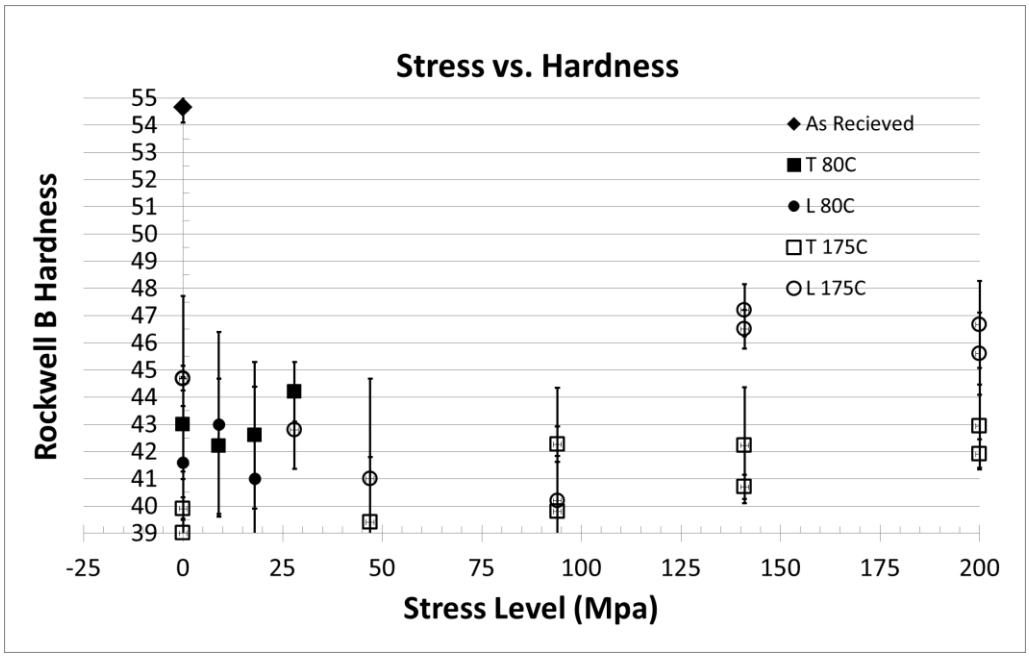

Figure 28. Data for Hardness Vs. Stress Level, Both 175°C and 80°C Sensitization Conditions

3. Etching of Grain Boundary β-Phase

Optical microscopy of the grain boundary β-phase did not show any significant relationship between stress and sensitization level. Optical microscopy of sensitized samples etched with phosphoric acid should show evidence of semi- or fully continuous β-phase at the grain boundaries in the case full sensitization. The etched microstructure of

the control sample showed no noticeable grain boundary Beta phase (Figure 29). The 80°C test condition samples formed β-phase, but it was discontinuous in distribution along the grain boundaries. There was also apparent β-phase formed in the interior of the grains. There was no distinguishable difference between the zero stress and stressed samples (Figure 30). For the 175C test condition samples, continuous β-phase was observed at the grain boundaries. There was an increase in the amount of β-phase which formed in the interior of the grains. The amount of beta phase formed was not apparently different the stressed an un-stressed samples (Figure 31).

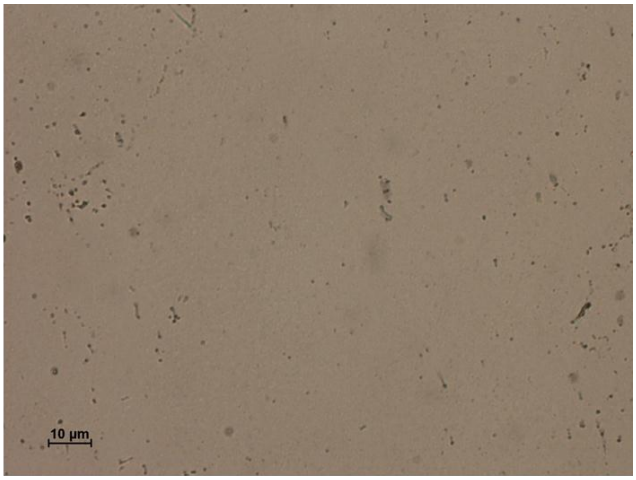

Image of LS 0 Mpa, Non-Sensitized

Figure 29. Optical Micrograph of Non-Stressed, Non-Sensitized Sample.

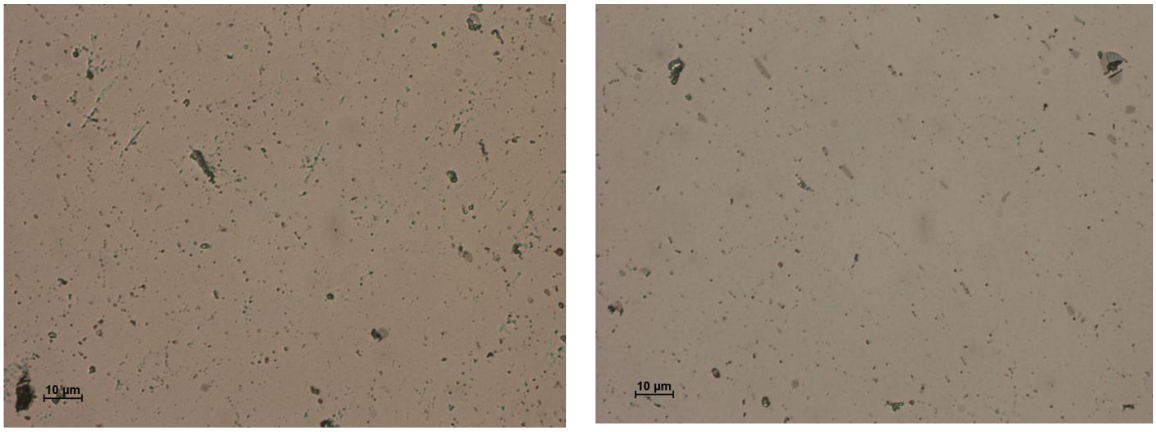

Image of LT 0 Mpa, Sensitization 80°C for 50 Hours

Image of LT 28 Mpa, Sensitization 80°C for 50 Hours

Figure 30. Optical Micrographs Comparing the Stressed (right) and Non-Stressed (left) 80°C Samples

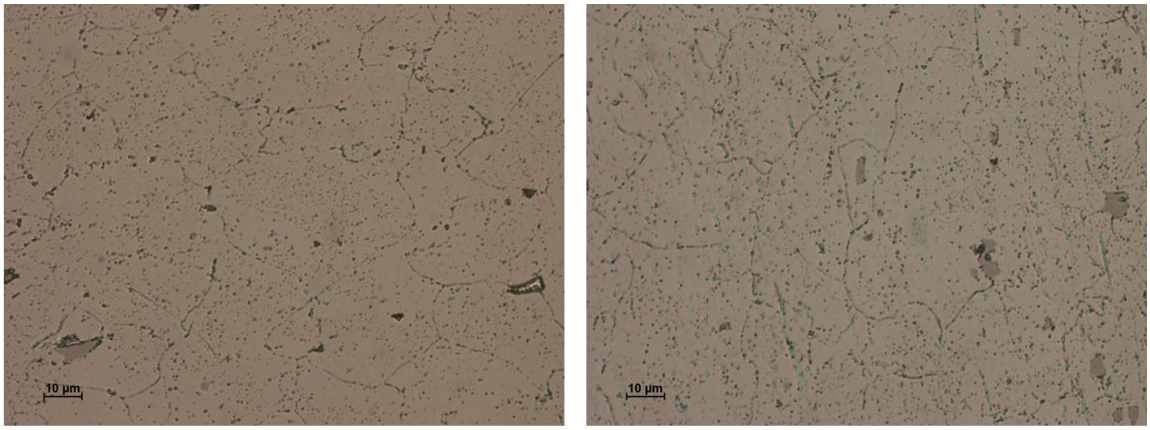

Image of LT 0 Mpa, Sensitization 175°C for 100 Hours

Image of LT 28 Mpa, Sensitization 175°C for 100 Hours

Figure 31. Optical Micrographs Comparing the Stressed (right) and Non-Stressed (left) 175°C Samples

C. PITTING NUCLEATION EXPERIMENT

Applied stress increased the rate of localized corrosion, both in terms of pitting and IGC. The stressed L and T samples had a greater amount of both pitting and IGC than the unstressed control samples (Figure 32-36). The unstressed L sample had the least amount of pitting and no IGC; there was no change in the amount of localized corrosion for the control sample between the 32- and 64-hour exposures (Figure 32). The unstressed L sample did have limited pitting corrosion on the sample (Figure 33). All samples had the same starting surface condition. In contrast, the stressed L and T samples

experienced significant changes in the samples' surface condition (Figures 34-36). The stressed L sample had a greater amount of both pitting and IGC than the unstressed sample, with total localized corrosion at 13/25 for the stressed sample and 12/25 for the unstressed sample of the same orientation (Figure 32 and 34). In the stressed L sample, while the amount of IGC stayed the same, the amount of pitting increased by 16% from the 32-hour to the 64-hour exposure times (Table 6). The surface condition of the T sample showed significantly more localized corrosion than was seen on the two L samples (Figures 32-36). The stressed T sample had 250% more IGC corrosion than the stressed L sample, while the amount of pitting was less, 9/25 vs. 13/25. The total localized corrosion was greater, 15/25, for the stressed T compared to 13/25 for the stressed LS. The stressed T sample also saw the greatest change from the 32-hour to the 64-hour exposures with the localized corrosion increasing by 24% (Table 6). The progression of IGC from the 32-hour to 64-hour exposures shows individual IGC expanding to form larger areas of corrosion that have the appearance of pitting (Figure 36).

32 Hour Exposure			
Condition	**Fraction Pitting**	**Fraction IGC**	**Fraction Localized**
L 0 MPa	12:25	0:25	12:25
L 100 MPa	13:25	3:25	13:25
T 100 MPa	9:25	8:25	15:25
64 Hour Exposure			
L 0 MPa	12:25	0:25	12:25
L 100 MPa	17:25	3:25	17:25
T 100 MPa	16:25	8:25	21:25

Table 6. Amount of Localized Corrosion in a 10 mm by 10 mm Area at 32 and 64 Hour Exposure Times

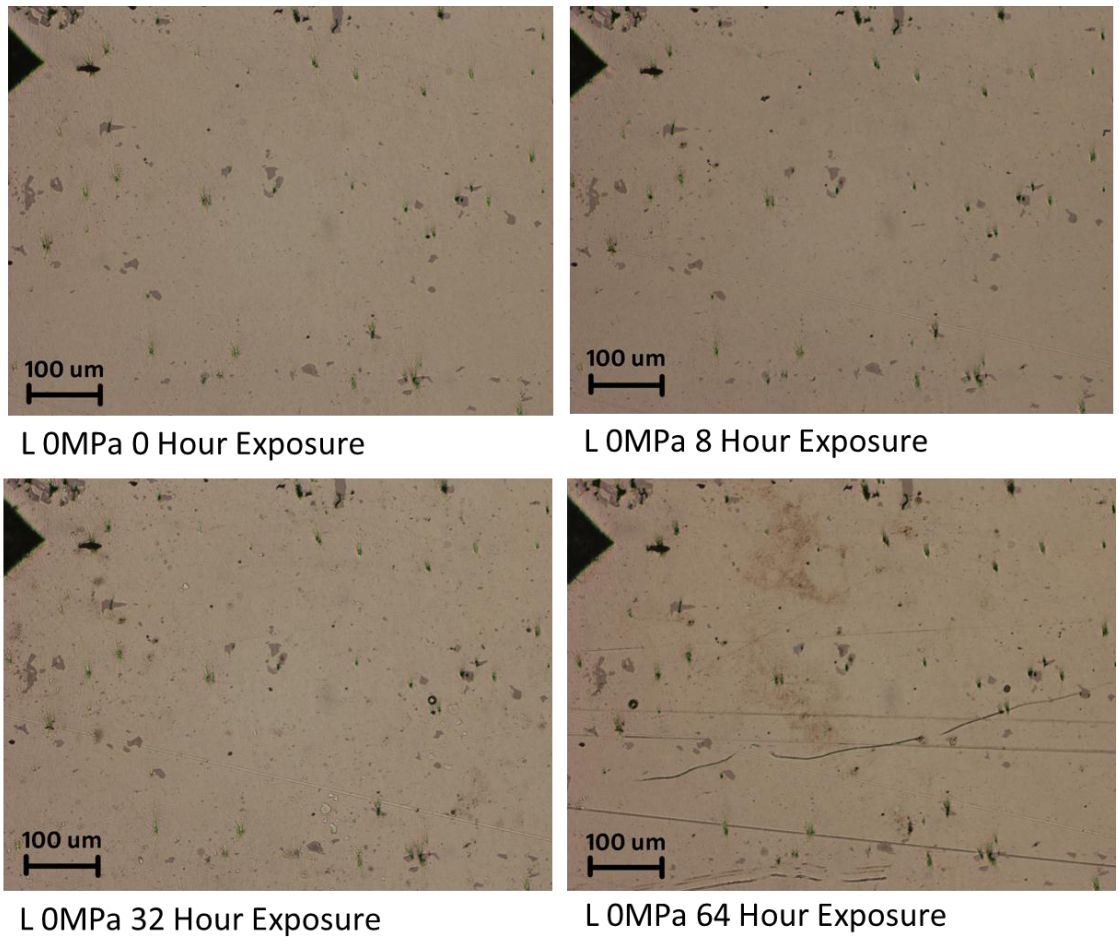

Figure 32. Optical Micrographs of the 0 MPa L Samples at 0, 8, 32 and 64 Hour

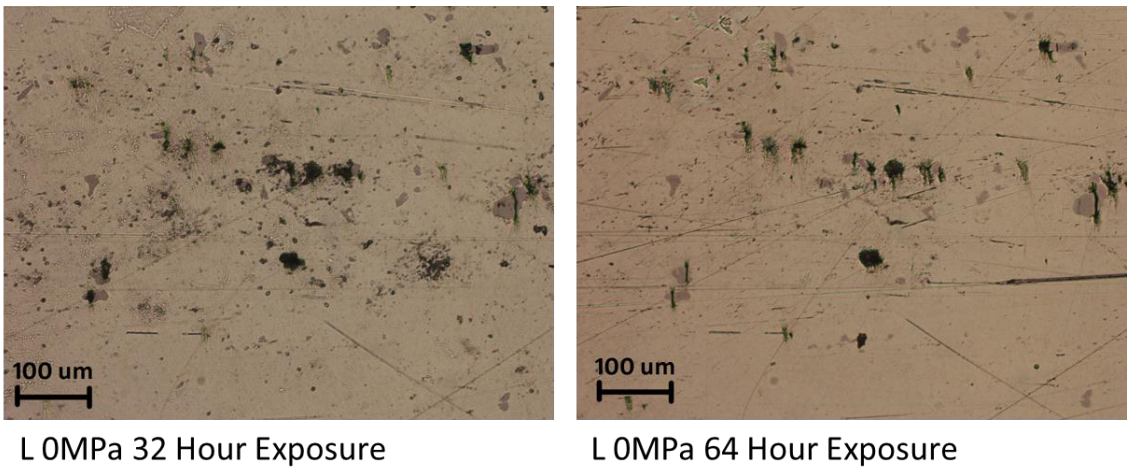

Figure 33. Optical Micrographs of the 0 MPa L Samples at 32 and 64 Hour Exposures, Showing Limited Pitting Corrosion

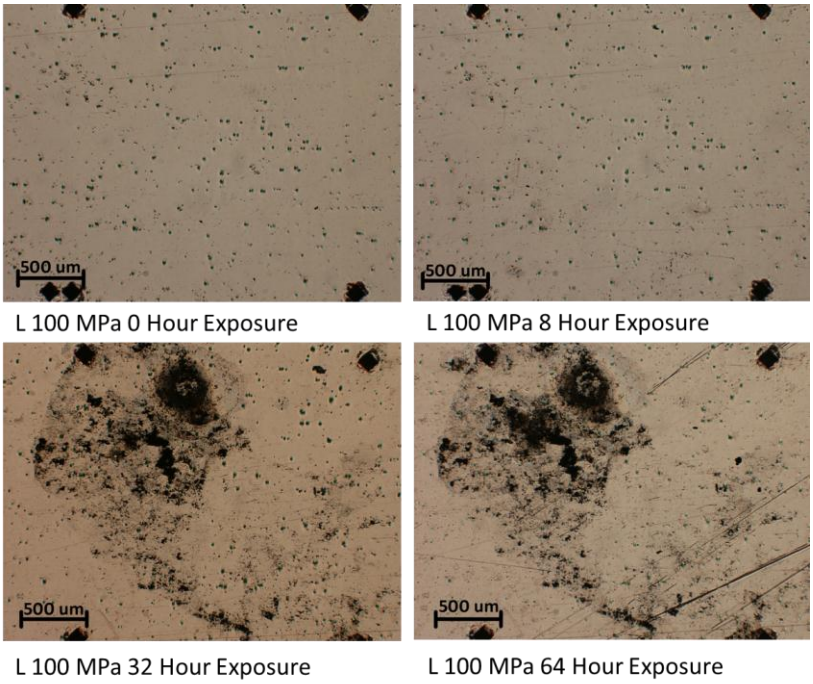

Figure 34. Optical Micrographs of the 100 0 MPa L Samples at 0, 8, 32 and 64 Hour Exposures

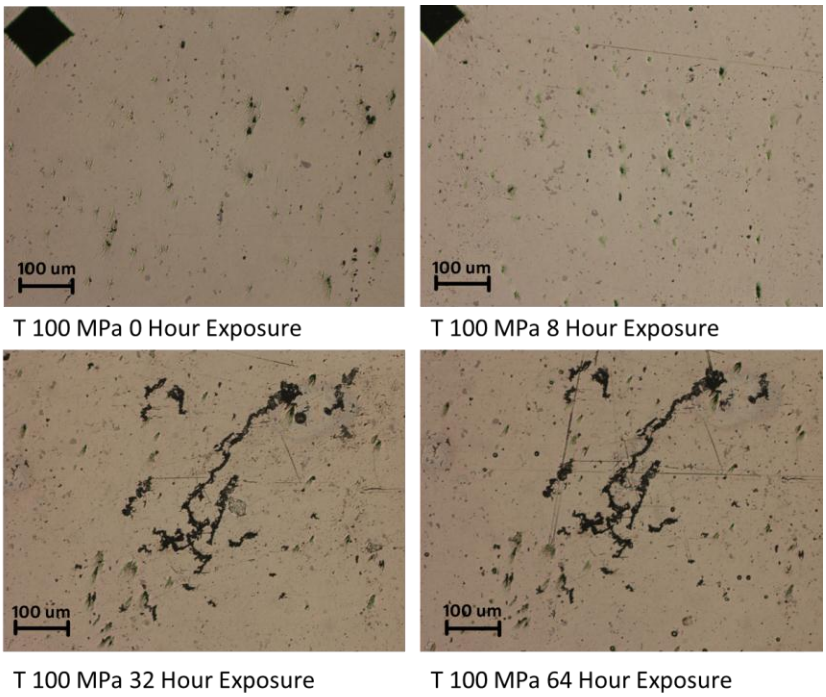

Figure 35. Optical Micrographs of the 100 0 MPa T Samples at 0, 8, 32 and 64 Hour Exposures

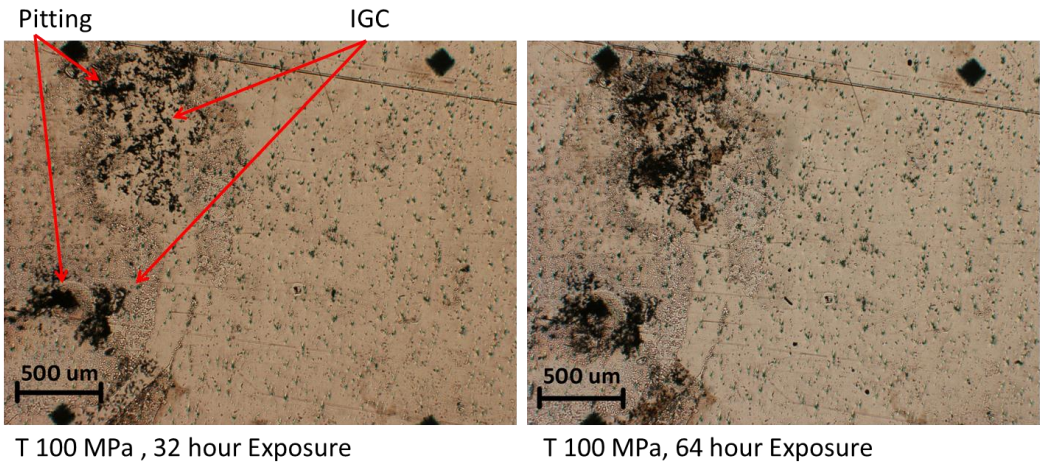

Figure 36. Optical Micrographs of the 100 0 MPa T Samples at 32 and 64 Hour Exposures, Showing Pitting and IGC

D. CRACK NUCLEATION EXPERIMENT

Even after exposure of 20 weeks, the bend samples did not fracture. In fact, no obvious visible cracks were nucleated in any of the samples tested. As was observed in the localized corrosion experiments, all samples had significant localized corrosion throughout the testing area. The samples, including the non-sensitized non-stressed sample, had evidence of both pitting and IGC (Figures 37, 38).

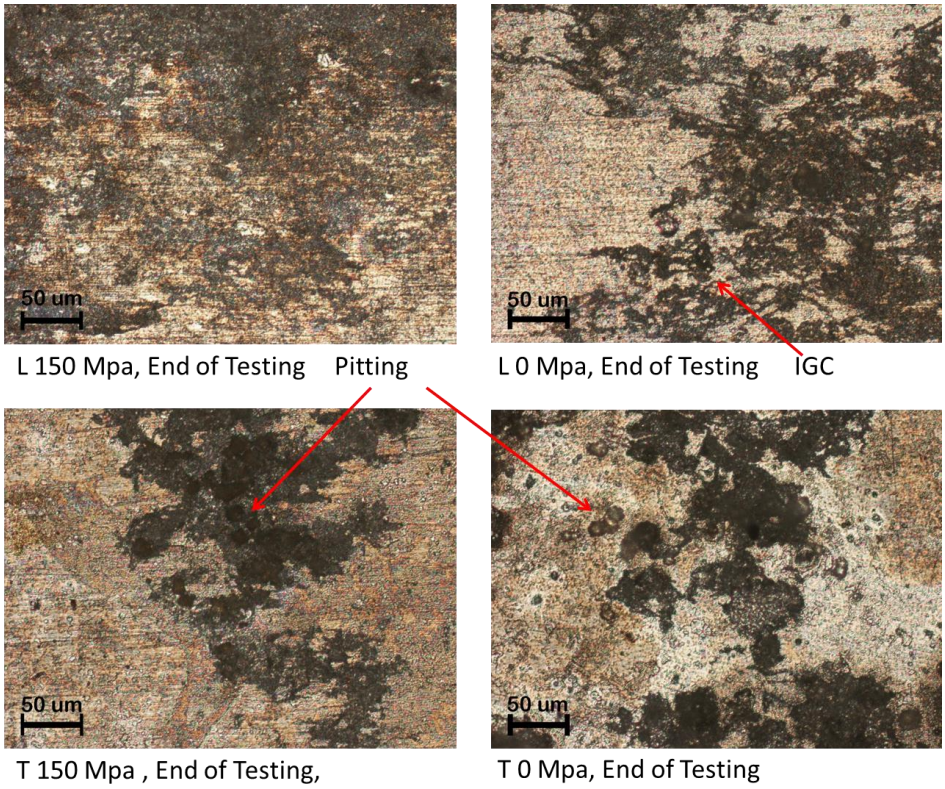

Figure 37. Optical Micrographs of Corroded Surfaces after 20 Weeks of Bend Testing

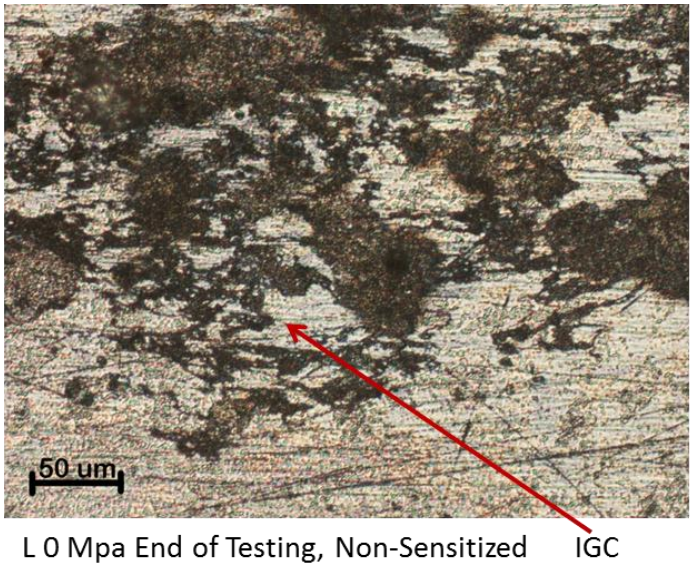

Figure 38. Image of the Non-Sensitized Crack Nucleation Sample

IV. DISCUSSION

A. THE EFFECT OF STRESS ON LOCALIZED CORROSION

The rate and type of localized corrosion is influenced by applied stress. The stressed samples showed more localized corrosion than the unstressed sample, indicating that the rate of localized corrosion is increased by application of a tensile stress. The results suggest that in the early stages of localized corrosion applied stress has a significant effect on the rate of localized corrosion. Work by Scully et al. showed that applying an electric potential the rate of IGC for 5083 drastically increases at a voltage of 0.73 V_{SCE}. From the current results, applying a stress instead of an electric potential has qualitatively the same effect of increasing the rate of IGC. In particular, IGC on the LT plane for 1 hour of exposure with an applied voltage of 0.73V, appears to be similar to that observed on the stressed T sample for an exposure of 64 hours with 100MPa of applied tensile stress, but with no applied voltage (Figure 39). Additionally the size and shape of the IGC is similar between the two samples [30]. The stressed L sample formed IGC and the unstressed did not, gives further support that the stress has a similar effect as an applied electric potential increasing the rate of corrosion (Figure 33 and 40). Additionally, not only did the stressed L sample show more IGC, but showed an increase in pitting as well over the unstressed L sample, this indicates that stress was increasing the total localized corrosion not just IGC (Table 6).

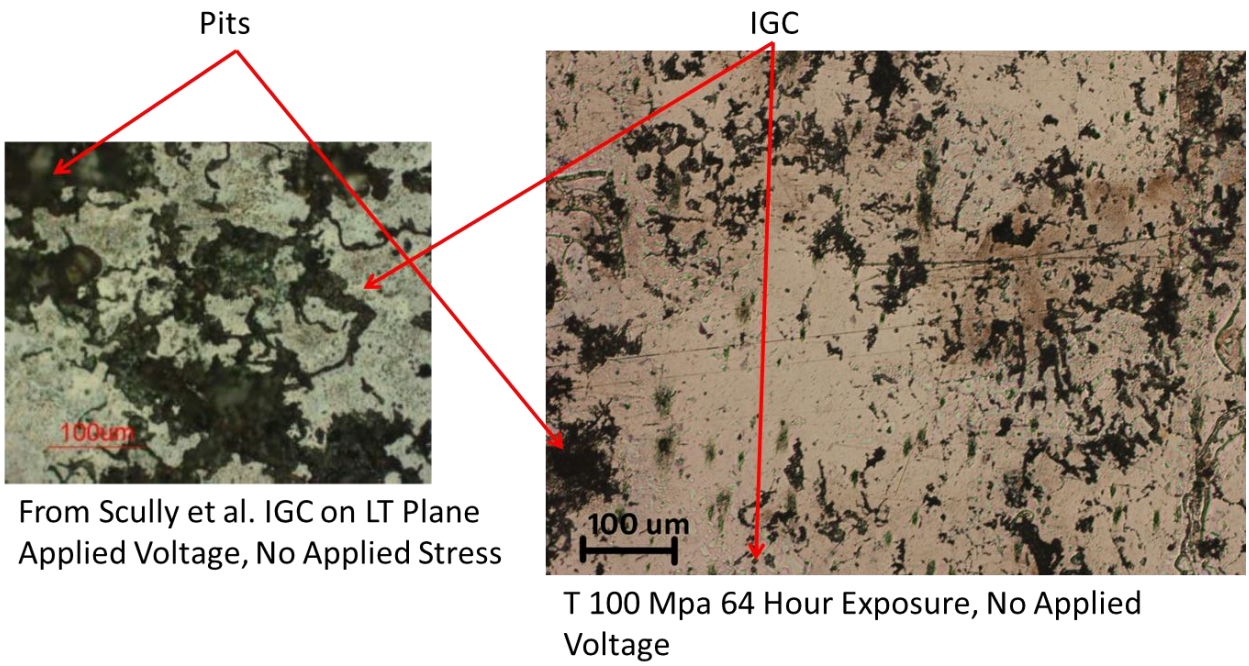

Figure 39. Optical Microscopy Comparing Results from Scully et al. and Stressed T Sample. From [7]

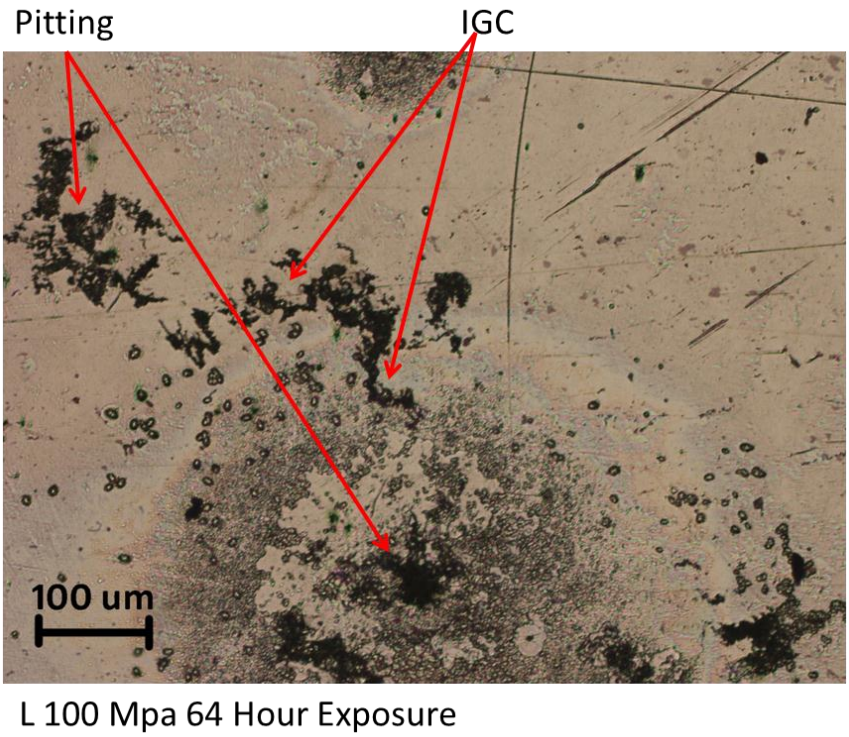

Figure 40. Optical Microscopy of L Sample 100 MPa, Showing Areas of Pitting and IGC

The orientation of the plate strongly influences the amount and type of localized corrosion. As expected from previous testing by Bovard et al., the T direction was more susceptible to IGC [8]. In the T direction, the applied tensile stress works to open up the grain boundaries, exposing them to salt spray and causing corrosion to proceed at a faster rate. In contrast, for the L direction, the applied, due to the Poisson's effect, actually closes the grain boundaries by means of a compressive stress. Taking this into consideration, it is not surprising then that the T sample had 2.5 times the amount of IGC than observed for the L sample. Scully et al. concluded that the IGC attack on the LT plane is greater because of larger clusters of particles and smaller grain diameter [7]. However, the fissures are parallel to the surface of the sample, which leads to exfoliation but not necessarily through thickness cracking. For IGC on the ST plane, the fissures are perpendicular to the surface (in the L direction), which does increase the susceptibility to through thickness cracking. Testing done in this thesis found that applying a stress on the LT plane in different directions (L and T) produced different rates of localized corrosion. Scully et al. determined that IGC is initially prominent around the constituent particles and then spreads to the grain boundaries. It is not possible to determine from the present results if the IGC initially starts at the constituent particles, however, looking at the micrographs taken before testing began show that the T sample had a greater number of intermetallic particles and particle fall out than the L direction samples. Greater particle density would allow for more sites where IGC could take hold that could be one of the mechanisms behind the greater amount of IGC seen in the T sample.

B. LIMITATIONS OF STRESS-SENSITIZATION EXPERIMENTS

The results of the sensitization experiments were severely impacted by the effects of creep. From the NAMLT results it is clear that there are no trends in the data for 175°C/100hrs condition. All of the samples tested had roughly the same sensitization level, upon further investigation it became apparent that the significance of creep had not been accounted for. The significance of aluminum's melting temperature is often overlooked. One of the sensitization conditions, a temperature of 175°C, is about 48% of the melting temperature of aluminum. When stress is present at temperatures around 175°C, the creep rate is high.

To calculate creep, a deformation mechanism map was used. The closest map to 5083 aluminum was a map for pure aluminum with a grain size of 10 microns, which was used for all creep calculations (Figure 41). The ratio of applied temperature over the melting temperature in Kelvin was calculated for both sensitization conditions used; 0.48 and 0.38 at 175°C and 80°C respectively. The applied stress, which is uniaxial only in one direction along the long axis, is normalized with the shear modulus. Using these two values, the strain rate (strain/S) was found using the deformation mechanism map. The number of seconds before the stress was relaxed in the sample was calculated by multiplying the applied strain by the strain rate. From the deformation mechanism map for aluminum (Figure 41), the time required before the stress relaxes is .014 seconds at 100 MPa and 5 seconds at 18 MPa. The creep effects are visually confirmed, as evidenced by the obvious bowing of the samples after being removed from the bending apparatus. Therefore, at the point when the aluminum has reached 175°C, the stresses have already relaxed, negating any effects stress would have had on the sensitization rate of the sample. For the 80°C test condition, the effects of creep are far fewer. At the 18 MPa stress level, it took 7.4 hours before the stresses relaxed. Although this was an order of magnitude longer, it was still very fast; the stress only affected the first 14.8% of the total sensitization time. For the aluminum subjected to 80°C for 50 hours, the 7.4 hours that it took for the stresses to relax was not sufficient time for the material to become sensitized to any significant degree. This result is shown by the NAMLT values for the 80°C samples, which have approximately one-sixth the amount of mass loss of the 175°C samples. The results show that as the temperature was lowered to reduce the rate of creep, the amount of sensitization was also simultaneously reduced.

With a stress level of 9 MPa, the time taken to relax the stress at 80°C was 372 hours. This duration of time allowed the samples to be subjected to a consistent load throughout the entire sensitization time. At this stress level, an increase in mass loss is shown in the NAMLT results. This result suggests that applied stress increases the rate of sensitization. However, the same result is not observed in the hardness and optical test results. This disparity can be attributed to the fact that since the 80°C samples are not very sensitized, the hardness and

optical tests are not sensitive enough to detect the differences between the stressed and non-stressed samples.

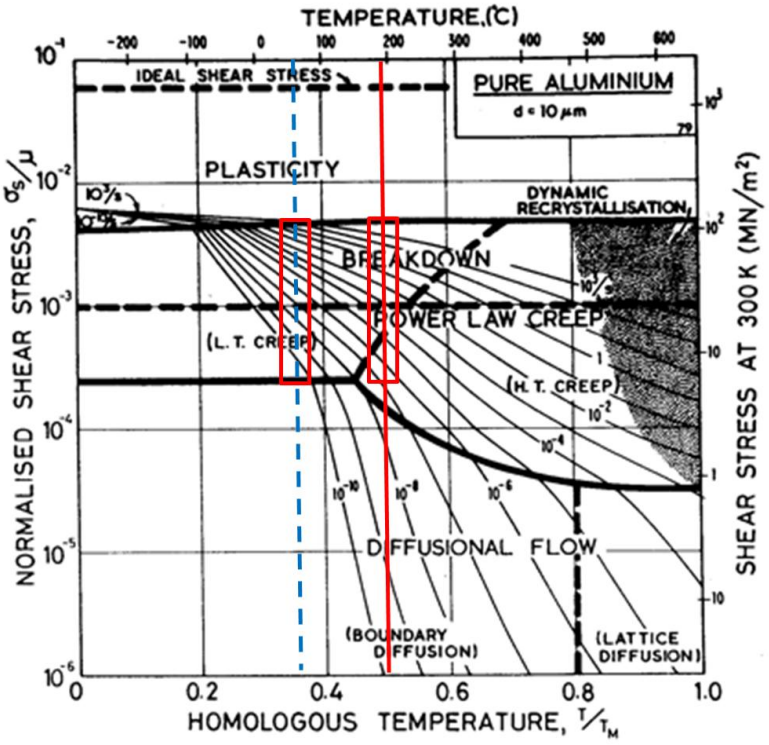

Figure 41. Deformation Mechanism Map, Red Line Designates T/Tm of 0.48, Broken Blue Line is T/Tm of 0.38 and Red Box Designates the Range of Normalized Stress Values. From [31]

One interesting result from the 175°C NAMLT data is that the zero stress samples had higher amounts of mass loss compared to the stressed samples both tensile and compressive. This result is likely an artifact of the sample geometries. The test specimens for the zero stress samples were twice the thickness of the stressed samples as they were not cut in half prior to the NAMLT test. While the ratio of the mass loss to the sample size should scale with surface area, the amount of mass loss is not consistent for all planes of the sample. While both specimens have the same amount of LT plane area, the thicker zero stress specimens have a larger percentage of the total surface area that is comprised of the LS and ST planes, directly exposing the grain boundaries to the acid. Looking at two typical zero stress and stressed specimens, there is 326% more LS and ST

surface area on the zero stress specimen compared to the stressed specimen. Furthermore, the ratio of LS and ST surface area to the total surface area is 32% and 13.5% for the zero stress and stressed specimens, respectfully. The surface corrosion difference between the thick and thin samples was confirmed by visual inspection of the specimens after completion of the NAMLT. The thicker zero stress specimens had noticeably more etching on the LS and ST planes than was seen on the LT plane, while the etching on the thinner stressed samples was significantly less. For the 80°C NAMLT all the specimens were made the same size and this effect is diminished. In summary, it is important to maintain the same relative areas of LT, LS, and ST planes on samples to be compared with NAMLT testing as the ASTM G67 specifies a range of sample sizes but does not specify that all sample have the same ratios of surface area types.

The values measured for NAMLT also showed sensitivity to temperature and the condition of the nitric acid used for the test. According to the ASTM G67, the temperature of the acid should be 30°C; however, there were no requirements outlined for temperature control [19]. Throughout the duration of the tests, it was apparent that the results of the test could be significantly affected by small changes in the temperature of the acid. A two- to three-degree centigrade change in acid temperature could move the mass loss numbers up or down by 10-30 mg/cm^2. It was also found that using a hot plate to heat the acid did not provide sufficient temperature control to keep a consistent temperature. During the course of the 24-hour test, the ambient temperature fluctuated, requiring a change in the heat input to the beaker. Since the hot plate was manually controlled, this was not possible. By using an feedback-controlled aquarium heater and increasing the amount of water used to heat the acid, a consistent temperature +/- 0.5 degrees was maintained. Also, covering the top of the aquarium with plastic helped to keep in the heat and significantly reduce the amount of water lost due to evaporation.

Another condition affecting the NAMLT was the age of the nitric acid. New acid that was not exposed to the atmosphere produced the best results. After the seal was broken on the acid bottle, the acid would yellow over a period of weeks, resulting in lower mass loss numbers than if a fresh batch of acid had been used. Ideally, fresh acid should be used for each test. In addition tests can be done with groups of specimens, so

that all the specimens would be tested at the same time, thus reducing the effects of the acid condition and temperature fluctuations.

C. CONNECTION OF CRACK NUCLEATION WITH SCC AND CORROSION FATIGUE

Cracks were not readily nucleated on the LT plane in AA5083. After 20 weeks of exposure no obvious cracks were nucleated in any of the samples, thus suggesting that cracks do not initiate easily from tensile loading on the LT plane. Work by Bovard, also showed this result uniaxial testing (ASTM G44/G49). There were no failures even after 6 weeks of exposure of sensitized AA5083 for samples loaded in the T direction at 75 percent of the yield strength. In contrast, sensitized samples uniaxially loaded in the S direction failed within 10 days for the same stress level at a sensitization of 33mg/cm^2. Sensitized samples with mass loss values of 44.2 mg/cm^2 failed when the stress was applied in the S direction within 24 hours [6].

There are several key differences in the choice of conditions for laboratory experiments that must be recognized. In traditional stress corrosion crack growth rate studies, Courtney et al. subjected samples to an air fatigue pre-crack in order to initiate a crack prior to stress corrosion crack growth testing as is standard for such testing. This step creates a well-formed, sharp crack and circumvents the more natural process of crack nucleation under static loading in a corrosive environment. In addition, the most susceptible orientations for SCC, SL or TL, were used for testing see (Figure 42). While these orientations crack easily in a laboratory environment, they are not representative of the common plate orientation in ship structures, biaxially loading in the LT plane. In addition, an electric potential was applied in order to speed up the cracking process. The work in this thesis used no applied potential, did not fatigue the sample to generate cracks, and cracks that formed would be in the LS or TS orientations; perhaps explaining the difficulty in nucleating stress corrosion cracks under a fixed displacement [7].

The role of cyclic loading on stress corrosion cracking must be further considered. Holtz et al. tested the effect of sensitization and either high or low load ratios with cyclic loading on the corrosion fatigue and IGSCC of AA5083 in the LT orientation. They

found that at high load ratios of R=0.85 and mass loss values of greater than 30 mg/cm^2 the corrosion fatigue properties were significantly degraded [32]. This work noted that the effects of cyclic loading on corrosion fatigue were more prominent for R=0.85 than R=0.1. Interestingly, as the R-value increases, the load spectrum more closely resembles monotonic loading with a small amplitude ripple on the load. They comment on the important interplay between SCC growth and corrosion fatigue. It is possible that SCC in the LS or TS orientations for sensitized AA5083 requires some cyclic loading to destabilize the passivating oxide film and to grow the small crack to dimensions at which SCC is self-propagating. This hypothesis should be borne out by future fracture tests.

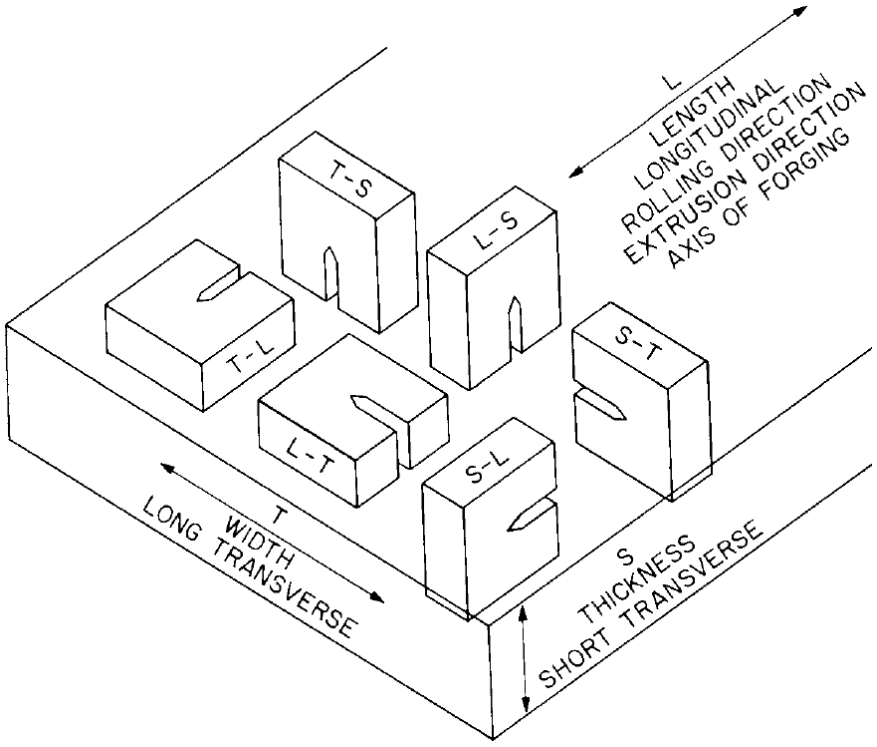

Figure 42. Crack Orientations for Rolled Plate Material. From [18]

V. CONCLUSIONS

1. Design, Build and Implement an Apparatus for Performing a Four-point Bend Test

A four-point bending apparatus was built and tested successfully. Experimental testing with strain gauges showed that the experimental values obtained closely matched the predicted values for strain.

2. Determine the Effect of Stress on the Rate of Sensitization of 5083 Aluminum

The effect of stress on the rate of sensitization is not clear. While, the NAMLT results from the 80°C test showed some evidence that stress was possibly affecting the rate of sensitization at the 9 MPa stress level, the other results were inconclusive. Hardness testing did not show any clear trends relating stress to the hardness of the samples. The hardness of all the samples was less than the as-received sample. There was no significant difference between the 80°C and 175°C hardness data. Optical microscopy did not show any significant difference in β-phase formation for the stressed and non-stressed samples. Under these conditions, applied elastic stress did not appear to have an appreciable effect on the rate of sensitization of 5083 aluminum.

3. Determine the Effect of Stress on the Rate of localized Corrosion of 5083 Aluminum

Applied tensile stress does appear to increase the rate of localized corrosion. The T-oriented sample had the greatest amount of localized corrosion and more than twice the amount of IGC as compared to an unstressed sample. The unstressed, L-oriented sample had no apparent IGC and the least amount of pitting corrosion. The stressed L sample had more pitting corrosion than the unstressed L sample, but less IGC than the stressed T sample.

4. Test the Effect of Stress on the Rate of Crack Nucleation in 5083 Aluminum

Surprisingly, the extended four-point bend test in a salt spray environment did not nucleate any apparent cracks in either laboratory or field conditions. As such, the results of the test are inconclusive as to the effect of stress on the rate of crack nucleation. The lack of fracture may point to the importance of cyclic loading on crack nucleation for these materials.

APPENDIX A. STRESS LEVELS FOR NAMLT

L/T	Stress Level (Mpa)
L	0
L	28
L	-28
L	141
L	-141
L	200
L	-200
L	47
L	-47
L	94
L	-94
T	0
T	141
T	-141
T	200
T	-200
T	0
T	28
T	-28
T	47
T	-47
T	94
T	-94
L	0
L	28
L	-28
L	141
L	-141
L	200
L	-200
L	47
L	-47
L	94

L	-94
T	0
T	141
T	-141
T	200
T	-200
T	0
T	28
T	-28
T	47
T	-47
T	94
T	-94
T	-18
T	0
T	-9
T	-28
T	0
T	18
T	9
T	28
L	0
L	9
L	-18
L	-9
L	0
L	18
T	-18
T	0
T	-9
T	-28
T	0
T	18
T	9
T	28
L	0
L	9
L	-18

L	-9
L	0
L	18

Table 7. Showing the Stress Levels used in NAMLT

THIS PAGE LEFT INTENTIONALLY BLANK

LIST OF REFERENCES

[1] R. H. Jones and R. E. Ricker, "Stress corrosion cracking," in *Stress Corrosion Cracking, Materials Performance and Evaluation*, 2 ed. Materials Park, OH: ASM International, 1992, pp. 347-365.

[2] R. Schwarting et al., "Manufacturing techniques and process challenged with CG47 class ship aluminum superstructures modernization and repairs," in *Fleet Maintenance & Modernization Symposium 2001: Assessing Current & Future Maintenance Strategies*, San Diego, 2011.

[3] H. Bushfield and M. Cruder, "Sensitized marine aluminum plate & ASTM standard specification B928-an update," in *SNAME Section Meeting*, 2006.

[4] I. N. Oguocha et al., "Effect of sensitization heat treatment on properties of Al-Mg alloy AA5083-H116," *Journal Of Materials Science,* vol. 43, pp. 4208-4214, 2008.

[5] F. S. Bovard et al., "Relevance of standardized tests and development of sensitization resistant 5XXX products," in *Workshop on Sensitization of Aluminum Alloy 5XXX Series*, 2011.

[6] R. Holtz et al., "Corrosion fatigue of Al 5083-H131 sensitized at 70,100, and 175^{o}C relation to microstructure & degree of sensitization," in *DoD Corrosion Conference*, La Quinta, CA, 2011.

[7] J. R. Scully et al., "Development and validation of an integrated intergranular corrosion/cracking model of Al-Mg alloys for naval applications," in *Workshop on Sensitization of Aluminum Alloy 5XXX Series*, 2011.

[8] F. S. Bovard, "Sensitization and environmental cracking of 5XXX aluminum marine sheet and plate alloys," in *Corrosion in Marine and Saltwater Environments*, T. T. D. A. Shifler, Ed., ed Pennington, NJ: The Electrochemical Society, Inc., 2005.

[9] R. Kelly et al., "Intergranular corrosion surface damage and penetration in Al-Mg alloys," in *ONR Workshop on 5XXX Series Aluminum Alloys*, 2011.

[10] S. Benedictus-deVries et al., "Fatigue crack initiation behavior of welded AA5083 in a seawater environment," *Journal of Engineering Materials and Technology*, vol. 126, pp. 199-203, 2004.

[11] J. L. Searles et al., "Stress corrosion cracking of sensitized AA5083 (Al-4.5Mg-1.0Mn)," *Aluminum Alloys 2002: Their Physical And Mechanical Properties Pts 1-3*, vol. 396-4, pp. 1437-1442, 2002.

[12] O. Hatamleh, P. M. Singh, and H. Garmestani, "Stress Corrosion Behavior of Peened friction stir welded 2195 aluminum alloy joints," *Journal of Materials Engineering and Performance*, vol. 18A, 2009.

[13] R. H. Jones et al., "Crack-partical interactions during intergranular stress corrosion of AA5083 as observed by cross-section transmission electron microscopy," *Scripta Materialia,* vol. 50, pp. 1355-1359, 2004.

[14] C. B. Crane and R. P. Gangloff, "Stress corrosion cracking of low temperature sensitized AA5083," University of Virginia, Charlottesville, Va.

[15] N. Dolić et al., "Pit nucleation on as-cast aluminum alloy AA-5083 in 0.01M NaCl,"*Journal of Mining an Metallurgy*, vol. 47, pp. 79-87, 2010.

[16] F. Zucchi et al., "Pitting and stress corrosion cracking resistance of friction stir welded AA 5083," *Materials And Corrosion-Werkstoffe Und Korrosion*, vol. 52, pp. 853-859, 2001.

[17] T. Trueba and S. P. Trasatti, "Study of Al alloy corrosion in neutral NaCl by the pitting scan technique,"*Materials Chemistry and Physics*, vol. 121, pp. 523–533, 2010.

[18] ASM International, "Standard test method for linear-elastic plane-strain fracture toughness KIC of metallic materials," vol. E399-09, ed. Pennsylvania: ASTM International, 2009.

[19] ASM International, "Standard test method for determining the susceptibility to intergranualr corrosion of 5XXX series aluminum alloys by mass loss after exposure to nitric acid," vol. G67-04, ed: ASTM International, 2004, pp. 1-3.

[20] N. Birbilis and R. Buchheit, "Electrochemical characteristics of intermetallic phases in aluminum alloys - An experimental survey and discussion," *Journal of Electrochemistry Society*, vol. 152, pp. B140-B151, 2005.

[21] R. H. Jones, "Stress-corrosion cracking," in *ASM Handbook*. vol. 13A, A. I. H. Committee, Ed., ed Ohio: ASM International, 2010, pp. 346-366.

[22] J. C. Farmer, "Stress Corrosion Cracking," in *MS3202 Lecture 13*, J. C. Farmer, Ed., ed. Naval Post Graduate School Monterey, CA, 2012.

[23] N. D. Green and G. A. Saltzman, "Effect of plastic defromation on corrosion of iron and steel,"*Journal of Corrosion-National Association of Corrosion Engineers*, vol. 20, pp. 294-298, 1964.

[24] A. R. Despic et al., "Mechanism of the acceleration of the electrodic dissolution of metals during yielding under stress," *Journal of Chemical Physics*, vol. 49, pp. 926-938, 1968.

[25] H. Krawiec et al., "Influence of applied strain on the microstructural corrosion of AlMg2 as-cast aluminium alloy in sodium chloride solution," *Journal of Corrosion Science*, vol. 65, pp. 387-396, 2012.

[26] X. F. Liu et al. "The influence of tensile stress on electrochemical noise from aluminum alloy in chloride media," *Journal of Corrosion Science*, vol. 51, pp. 1460-1466, 2008.

[27] B. Liu et al., "Effect of hydrostatic pressure on the corrosion behavior of pure nickel,"*International Journal of electrochemical science*, vol. 7, pp. 1864-1883, 2012.

[28] L. Kramer et al., "Locally reversing sensitization in 5xxx aluminum plate," *Journal of Materials Engineering and Performance*, vol. 16, 2007.

[29] ASM International, "Standard practice for preparation and use of bent-beam stress-corrosion test specimens," vol. G39-99, ed: ASTM International, 2011, pp.1-8.

[30] J. R. Scully et al., "Spreading of intergranular corrosion on the surface of sensitized Al-4.4Mg alloys: A general finding," *Corrision Science*, vol. 59, pp. 136-147, 2011.

[31] H. J. Frost and M. F. Ashby. (2013). *Deformation-Mechanism Maps, The Plasticity and Creep of Metals and Ceramics* [Online]. Available: http://engineering.dartmouth.edu/defmech/

[32] R. L. Holtz et al., "Corrosion-fatigue behavior of aluminum alloy 5083-H131 sensitized at 448 K (175°C),"*Journal of Metallurgical and Materials Transactions*, vol. 43A, pp. 2839-2849, 2012.

INITIAL DISTRIBUTION LIST

1. Defense Technical Information Center
   Ft. Belvoir, Virginia

2. Dudley Knox Library
   Naval Postgraduate School
   Monterey, California

3. MAE Department Chairman,
   Dr. Knox Millsaps
   Naval Postgraduate School
   Monterey, California

4. Engineering and Technology Curricular Office, Code 34
   Naval Post Graduate School
   Monterey, California

5. Professor Luke N. Brewer
   Naval Postgraduate School
   Monterey, California

6. Professor Young Kwon
   Naval Postgraduate School
   Monterey, California